IJRAR.ORG   E-ISSN: 2348-1269, P-ISSN: 2349-5138

INTERNATIONAL JOURNAL OF RESEARCH AND ANALYTICAL REVIEWS (IJRAR) | IJRAR.ORG

An International Open Access, Peer-reviewed, Refereed Journal

Vibration Analysis of Crack Developed Bridge Using ANSYS

By: - Barkha

CHAPTER- 1

INTRODUCTION

1.1   Overview of Bridges

Designers understand that all constructions are a part of the infrastructure and that they all work around each other. Bridges plays a vital role in connecting diverse regions by spanning over cliffs, rivers, lakes, & valleys. Bridges are critical components of land transportation infrastructure because they link otherwise inaccessible regions. The designers of a river crossing bridge have several vantage points from which to choose [1].

a. A city dweller may envision the bridge as an easy way to get to schools, parks, as well as theatres, or as an easy manner to visit a relative.

b. A designer or interior designer envisions the bridge as a means of connecting the road to multiple city locations, like health facilities or fire departments.

c. From the point of view of the business community, the bridge provides access to numerous regions for trade, goods distribution as well as facilities.

The significance of a bridge will indeed base on the requirements of the society. A bridge that links two city points as well as provides as a direct link to recreation areas has a lesser impact than a bridge that crosses a large river as well as linking the two city marks with a high flow of traffic [2]. Considering the preceding sentence, designers recognize that bridges are not built arbitrarily; extensive preparation, such as design, building, operation, and preservation of the constructions, is required.

1.2   Reasons for Bridge as Key Elements in Transportation [1]

1.2.1   Capacity control

i.   **Bridges should meet traffic flow specifications all through their service life.**

A bridge could indeed keep a constant vehicular flow if it has a limited lane numbers, narrow dimensions, or limited space.

ii.   Bridges should withstand the necessary loads throughout their service life.

This implies that the assessment as well as architectural engineering must account for all of the huge amounts that the tower should withstand. In the event that a structure is situated along an interstate highway, yet lacks the capacity to accommodate heavy-duty truck loads, it will experience restricted vehicular movement, thereby impeding the passage of large trucks across the bridge. Consequently, alternative routes will need to be sought by truckers to reach their intended destinations.

1.2.2   High expense for the entire road network

i.   Bridges account for a significant portion of road expenditures

In terms of cost per kilometre, planners find that building a bridge is far more costly than building a motorway.

ii.   High-cost variance across bridge geometrical.

The expense of the bridges differs determining on the set of lanes acquired, the kinds of vehicles to be aided, the ranges or clean time to cover, the substances used, & the way to offer. To fulfil the requirements while remaining within the budget, proper planning is acquired.

1.2.3   The bridge is an element of the system

i.   The whole road system is at risk if the bridge gives way. If researchers evaluate the whole roadway and one bridge collapses at a given spot, traffic will rise, delays will occur, time will be wasted, and an alternative route would be necessary.

ii. Alternative routes would be impacted if the bridge is not operational. When a bridge fails, people who use the impacted road must take an alternate path, which is likely not constructed for an immediate enhanced in vehicular flow, resulting in time wasted, large distances, as well as extra fuel usage.

1.3   Ancient bridges:

Bridges were originally created with simple geometry and had extremely specific applicability as they only travel very short times, including small rivers. These bridges were built with simple materials like stones, ropes, wood etc. [1].

1.3.1   Stone arch bridges:

The stone arch was the first new bridge using mathematical techniques. The actual date of building works is unknown, but there are buildings formed through civilizations like the Greeks & Romans that used this form of bridge as aqueducts, roads for pedestrians, as well as carriages. The utilisation of the compression strength of rock, derived from its shape, is a characteristic feature of stone arch bridges, as illustrated in Figure 1.1. This design enables them to bear the weight of both live loads and their own structure. The structural integrity of these buildings is often reinforced by the arches, which provide support for the levels situated above them. This specific bridge resembles both the "Pont Du Grad Aqueduct" in France and the "Segovia Aqueduct" in Spain. The first and second centuries saw the construction of both buildings.

Figure 1.1 Bridge with stone arch design [3]

1.3.2 Wooden and steel truss bridges

Through the early 19th century, wood was widely used in construction, but also truss bridges started appearing (Figure 1.2). These wooden trusses gained control of the bar components' axial stress ability, resulting in bridges with larger diameter, reduced mass, sufficient rigidity to handle heavier pressures. Because trusses may be used to create such a wide variety of geometries, there are many different ways in which the bar components might be organised to maximise their resistance to tension and compression. A few instances are as follows:
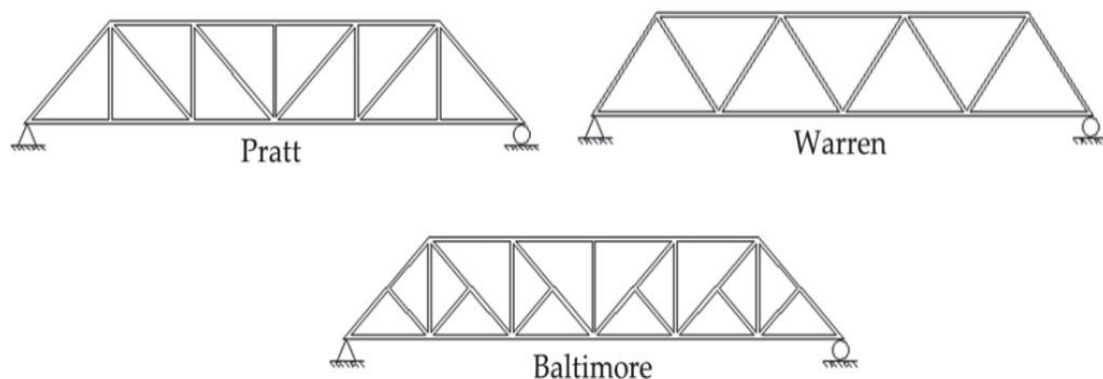
Figure 1.2 Geometry and Kinds of trusses [3]

1.4 Modern bridges

With the advancement of the industry sector in the mid-nineteenth century, vehicles as well as trains began to circulate using the current transport network. As a result, more roads, railroads, as well as bridges were constructed to meet the increased traffic demands.

1.4.1 Steel truss bridges

Since its rise in flow as well as vehicle weight began, wooden bridges have been unable to handle these vehicle loads, as well as constructions have begun to use structural steel. With the availability of stainless components on the construction sector, these bridges improved significantly, consisting a rise in span length protected as well as the capacity to handle higher loads as illustrated in fig. 1.3.

Figure 1.3. Scotland's Edinburgh and the Forth Bridge [4]

1.4.2 Suspension bridges

The innovation of the suspension bridge marked a significant progression due to its capacity to span vast distances. The deployment of grandiose structures of this magnitude functions as a symbol of the urban centre, concurrently leaving a lasting impression on its guests. "The Brooklyn Bridge" in New York and the "Golden Gate Bridge" in San Francisco are two fantastic examples of bridge design. The suspension bridge is composed of a deck, girders, and subsidiary cables that are situated above the main cables, with two towers located at its centre. The cables provide support to the primary deck, which experiences a significant volume of traffic and serves as a source of stress for the overall structure. Suspended bridges are capable of achieving significant spans without the need for intermediate supports due to the conspicuous visibility of tension wires. They are frequently employed in locations where conventional bridges are not feasible, such as spanning significant bodies of water. The aerodynamic homogeneity of these frameworks is compromised by many factors, including the thin main slab, the size of the span clearance, and the participation of propulsive forces produced by wind-induced stresses.

Figure 1.4. Suspended Golden Gate Bridge in San Francisco, California, U.S.A. [5].

1.4.3   Pre-stressed, post-tensioned, and reinforced concrete bridges

As a result of Portland cement's widespread availability and the growth of concrete construction technology, reinforced-concrete building design assumptions were created in the early 1900s. Long-span bridges are typically built using reinforced concrete and feature an arch located beneath the primary superstructure. The structure is primarily composed of columns that provide support for the main superstructure and a lower arch. With the exception of the primary deck, all components of the bridge operate under compressive forces. These bridges advantage from the material's compression capacity while avoiding tension elements. The majority of today's bridges have short and medium spans, which makes them ideal for connecting cities via highways and roads. In these situations, girder-based frameworks with easy or constant assistance are commonly utilised.

Figure 1.5: Bridge of pre-stressed concrete Girders el Zacatal, México [6].

The suitability of girder-based structures may be limited in comparison to beams, owing to the bending capabilities of girders. The fabrication of girders is a relatively uncomplicated process, and the evaluation of costs and benefits renders such architectural configurations financially feasible. Figure 1.5 depicts the El Zacatal Bridge in Mexico, which is built with pre - stressed concrete girders.

1.5   Degradation process: corrosion, wear and fatigue

Because geological and physiological elements exist in each framework, all components could well be affected by chemical composition changes, adjusting mechanical characteristics, lowering the useful life of the building as well as necessitating the use of repair and service. This part contains the variables that have changed.

1.5.1   Corrosion

Corrosion is a chemical process that occurs when structural concrete and steel reinforcing steel are exposed to moisture. This process involves an electrochemical reaction triggered by direct contact with moisture, ultimately leading to rust formation and the gradual deterioration of the material.

When reinforcing steel bars used in concrete get exposed to oxygen, a process known as corrosion may set in. Corrosion of the reinforcing steel is shown in Fig. 1.6 as the source of a damaged pier, which has lost its covering and had its cross-sectional area reduced, indicating a drop in mechanical capability. If the stainless system is completely opened for the surroundings without any moisture safety, the tier of combustion would

be visible throughout the component & therefore would cause a generalised rusting response. Figure 1.7 illustrates a structural steel bridge with all components rusted.

Figure 1.6. Cement reinforced metal piers with corrosion issues [7].

Figure 1.7. Corrosion issues on a structural steel bridge [8].

1.5.2 Wear and Fatigue

During the bridge's daily operation, corrosion occurs due to mechanical forces, such as the friction generated by vehicles traversing the main deck. When these automobiles brake as well as accelerate, frictional forces are generated, causing wear on the structure. Friction causes the degradation in bridges where the piers come into the connection with flowing water. The degradation of decks caused by vehicular traffic is typically of a minor nature. However, in cases where the road is defective, the wear and tear, as well as collisions, may expedite the deterioration process, leading to significant impairment. Girder bridges of basic design require

joints at the junctures where the girders meet the supports. These joints serve as noteworthy illustrations of areas where substandard manufacturing methods may result in defects.

Figure 1.8. bridge concrete construction joint Cracked [9].

Diagram 1.8 depicts a common bump issue that can be prevented by using any joint process as well as materials available in the market place. The excessive strain on certain sections of the bridge is resulting in fatigue due to the high volume of vehicular activity, thereby presenting an additional physical challenge. The mechanical characteristics of a material deteriorate with successive loading cycles as a result of wear. This implies that the mechanical characteristics of each vehicle that completes the race deteriorate compared to their initial state. If the stress generated by each cycle is equivalent to or surpasses the original stress of the material, the material may experience degradation and consequent weakening after a significant number of cycles. Diagram 1.9 depicts a fracture that resulted from cyclic loading. It should be noted that the beam exhibited a brief fracture and was devoid of any additional fragments.

1.6   Finite Element Method

The finite element method is a useful numerical technique for problems that may be characterised by partial differential equations or phrased as functional minimization. An area of interest is shown here as a collection of discrete elements [7]. The nodal values are determined for physical fields. The physical problem which is continuous are converted in to discretized problem where in the nodal values are unknown.

1.7   The general procedure of finite element method

The procedure of FEM involves 3 different stages. These stages are:

- **Pre-processing:** Subsequent to the development of a CAD element, the subsequent phase involves preliminary measures such as mesh generation, loading, and the establishment of boundary conditions.

- **Solution:** As part of finding a solution, a global stiffness matrix and a local stiffness matrix are generated. The identification of nodal discoveries is achieved through the inversion of the matrix and its subsequent multiplication by itself.

- **Post-processing:** The post-processing stage involves viewing results which include vector plots, contour plots and streamline plots.

1.8   Advantages of FEM

The FEM offers various advantages as compared to experimental techniques. The 1st advantage of FEM is easier analysis of complex shapes which are irregular.

Here are six advantages to this technique:

- ➤ **Modeling.** The complex irregular shapes and geometries can be easily developed and analyzed. The critical regions of high stresses and other geometric factors affecting the results can be evaluated.

- ➤ **Adaptability.** The design cycle and cost of production can be reduced significantly as it reduces number of iterations. The hard-prototyping stage can be removed.

- ➤ **Accuracy.** The precision of the result may be enhanced by using convergence methods and doing more iterations.

- ➤ **Time-dependent simulation.** The transient structural analysis, transient thermal analysis can be conducted on different structures.

- ➤ **Boundaries.** The user can change boundary conditions easily as compared to experimental techniques. The thermal, structural and fluid flow conditions are easily changeable.

- ➤ **Visualization.** The FEA simulation package enables user to identify regions (critical regions) of high stresses, deformation and safety factor.

1.9   Limitations in FEM

Despite the relatively slower response time of Finite Element Method (FEM), it yields more precise outcomes in cases where the underlying phenomenon can be determined through coefficients or cloth qualities. The primary method of partitioning the error-free process into computational entities is considered to be one of the most laborious aspects of utilising FEM's software.

1.10   Applications of FEM

1. **Mechanical engineering:** In automobiles component design, machine component design and other tool design.

2. **Geotechnical engineering:** The geotechnical engineering involves soil stability, soil structure and fluid solid interaction. The analysis involves heavy structures like tunnels, dams etc.

3. **Aerospace engineering:** The aerospace engineering involves use of FEA in aircraft design, shuttle design. The type of analysis involves vibration and structural type.

4. **Nuclear engineering:** The safety and performance of nuclear reactor is investigated. The analysis of reactor involves steady state and transient state.

CHAPTER- 2

REVIEW OF LITERATURE

2.1   Background

Priyanka Dilip P. and Fahad P. P. [2017], An obvious bridge segment called a box girder bridge has major longitudinal girders that are arranged in the form of hollow boxes. The box girder is made of steel, concrete that has undergone prestressing, reinforced concrete, composite materials, or any combination of these. Box girders often have rectangular, square, and trapezoidal cross sections. This study evaluates and plans for a 240-meter-long, two-lane bridge. A trapezoidal section of a two-cell post-tensioned box girder bridge is examined under various design loads in accordance with the IRC Code for Loads and Load Combinations (IRC:6-2014). Superimposed dead loads, dead loads, moving loads, prestressing force, and so on are all covered by this code. The post-tensioned box girder bridge is analysed using SAP 2000 version 19. Tension anchors are installed using the Freyssinet technology [2].

Phani Kumar, S. V. V. K. Babu, and D. Aditya Sai Ram [2016], In the construction industry, bridges that link highways, roads, and railways throughout the globe are very important. Prestress girder bridges are quite common in the area of bridge engineering because they are more reliable, affordable, structurally efficient, and have a pleasing look. Prestressed concrete box girder and T-girder bridges are analysed and designed in this thesis. In order to analyse the bridges, IRC:112-2011 is used. IRC:112 is a code of a more recent generation. The new code's design guidelines vary from those in earlier codes. Prestressed concrete buildings must adhere to IRC:18 whereas reinforced concrete buildings must adhere to IRC:21. The primary distinction between IRC:21 and IRC:112-2011 is that the former is based on the limit state approach while the latter two are based on the operational stress method [3].

Sanket Patel and Umang Parekh [2016], Since the dawn of human history, bridges have been used for a variety of reasons. Since the beginning of time, many bridges of all shapes and construction materials have been erected. A careful choice of structural components must be made in the earlier stages of medium span highway bridge design. The primary objective of this research is to provide a practical user interface for the early stages of bridge system design. Only by evaluating a small number of designs can the most cost-effective design be discovered. To discover the most economical design, a certain set of criteria might be applied. Depending on the circumstances, it may be necessary to take into account more than one of the following criteria in order to achieve optimal efficiency: The cost of prestressing steel, concrete usage, superstructure cross section, and span. The bridge superstructure of prestressed concrete girder bridges has been analysed parametrically[1].

Pragya Soni, [2017], The act of bridging predates the development of human civilisation. Since the beginning of time, many bridges of all shapes and materials have been constructed. A medium span highway bridge system's first design process requires careful structural element selection. To provide some helpful interface for the early design of a bridge system is the goal of the current work. The only way to determine the most cost-effective design is to compare a few distinct ideas. The most economical design may be found under a certain set of circumstances. Accounting for the span, the cross section of the superstructure, the price of the

prestressing steel, and the amount of concrete used may all help to achieve economy. In the present study's parametric analysis, the superstructure of the prestressed concrete girder bridge is taken into account [10].

Jagdish Chand, Ravikant [2019], The path sometimes may be blocked or obstructed by a river or valley. Consequently, a route or passage is created across the barrier or obstacles without disrupting the alignment. This research focuses on the design of bridge girders, both longitudinal and transverse. The girders for the bridge spans are all 25 metres in length. Dimensions of 2000x500mm for cross girders and 1500x250mm for longitudinal girders are anticipated. Three longitudinal girders are planned to be placed at 2600 mm c/c on the shorter route and 5000 mm c/c on the longer route. The STAAD Pro programme is used to create girder designs. Three identical models are created in STAAD Pro for bridge girder analysis, and IRC, Euro, and AASHTO loadings are used. According to these various loadings from both longitudinal and cross girders, shear force, bending moment, and steel area are calculated from the models. When the analysis is complete in STAAD Pro, the results are shown in tables and graphs for comparison [4].

R. Shreedhar and Spurti Mamadapur [2020], The use of I.R.C. loadings allowed for the one-dimensional analysis of a straightforward T-beam bridge with one span. STAAD ProV8i, a bridge analysis programme, analyses a T-beam bridge by means of finite element plates representing the primary beam and deck slab of the bridge. As a 3D structure, the single span of the bridge is examined. The models are examined under different IRC loadings. In order to generate responses, shear force, and maximum bending moment, both models are loaded with I.R.C. Manual calculations are more cautiously conducted and are subject to IRC loadings. When compared to the finite element model, one-dimensional analysis yields more results. T-beam bridge decks are a significant and often used concrete bridge deck type among the many various kinds of bridges. The bridge deck is a cast-in-place kind. The decks of T-beam bridges are made up of monolithically joined concrete slabs and girders. The analysis of a group of finite elements is used to approach a problem's solution in continuum mechanics. This method is used to describe the problem's solution domain and involves the coordination of finite elements at nodes of finite number. Finite element analysis (FEA), a common tool in structural analysis, is utilised to investigate this [5].

T. Sujatha, Y. Yadu Priya [2016], Better live loads may be carried by pre-stressed concrete bridges. Pre-stressed concrete bridge decks are becoming more often used in the area of bridge engineering. IRC bridge codes are used in the study. In the research, IRC provisions are used. One of the most well-liked and often used types of cast-in-place concrete decks is T-beam bridge decking. They are totally constructed of slabs of concrete. Girders are given for T-beam bridge decks. This technique substitutes a comparable idealised structure for the real continuum. The standard technique for analysing the structure is STAAD Pro. These two lanes, single span t-beam bridge is examined. Where the width is held constant, various spans are taken into account. The spans that are taken into consideration are 25 metres, 30 metres, 35 metres, and 40 metres. The bridge is put through its paces using the IRC class AA and IRC 70R tracked loading system, which applies the most extreme reactions, bending moment, and shear force possible. The findings show that the bending moment and shear force on the girder both rise as the span lengthens [6].

Sharu. E, Nivedhitha M and Gowtham Raja M [2018], A bridge is a constructed structure that facilitates the traversal over a valley or obstacle while maintaining the cleanliness of the space underneath it. The pathway may include several forms of infrastructure, such as a designated pedestrian walkway, a thoroughfare for vehicular traffic, a railway track, a waterway in the form of a canal, or even a natural depression like a valley. Many bridges fall across the globe for a variety of causes. However, poor design is the main cause of bridge collapse. As a result, correct designing is necessary. Using the R.C.C. T-BEAM Bridge correctly. In order to properly develop a design, they relied on established practises, standard code books, and prior study. how far the bridge with three lanes stretches. The reinforcement's transparent cover is estimated to be 40mm thick. All of the bridge's parts are constructed with IRC loadings in mind. This includes the Bearing, pier cap, pile cap, abutment, girders, and deck. These components were created using IRC loadings, and they are being tested with real loading. The bridge's ability to withstand earthquakes has also been examined. Finally, we are at the point where the T-beam Bridge is overflowing due to the present traffic situation [7].

Prof. R.B. Lokhande, Abrar Ahmed [2017], In order to promote appropriate mobility, flyovers and bridges must be built since agricultural & industrial activity are the key drivers of the country's growth. Construction of flybys & bridges often uses T-beam & box type sections. The objective of this project is to choose the best section by comparing the cost, design, and analysis of the T-Beam & Box girders with equivalent spans. The goal of this book is to identify the most appropriate and cost-effective section for various span bridges [8].

Sudip Jha, Cherukupally Rajesh, P.Srilakshmi [2015], Since agricultural and industrial operations account for the majority of the nation's growth, bridges and flyovers are necessary to provide effective mobility. Flybys & bridges are often built using T-beam and box type sections. This study compares the time and money spent on analysis and design for T-Beams and Box girders for the same span. The primary objective of this work is to provide guidance to designers in the selection of the most optimal and economically viable cross-sectional configurations for bridges with different spans [9].

Chen et. al. [2018] In this research, a three-dimensional bridge mechanism is built and analysed. The mechanism proposed in this research not only shares the space-saving, easy-to-build, symmetrical design, and other advantages of conventional bridge-type mechanisms with their predecessor, but also significantly outperforms them in terms of amplification ratio. This research proposes a new assessment measure called relative amplification rate for calculating the amplifier's displacement loss. A theoretical framework is constructed to analyse the rate and ratio of relative amplification, using the principles of screw theory. In this study, we assess and analyse several bridge-type mechanisms that are linked to four conventional flexure hinges. Our evaluation is based on a previously published mathematical model, and we also account for the distribution of stiffness in our analysis. The V-shaped hinge and the filleted leaf hinge were used in the study. The obtained numerical findings indicate that the bridge-type mechanism under investigation exhibits significant amplification ratios and relative amplification rates for bridges 1 and 2, respectively. Ultimately, the performance of the amplifier is confirmed by the use of FEA modelling and testing. This validation process demonstrates that the amplifier successfully achieves a 41:1 amplification ratio and a relative amplification rate of 0.93:1 [11].

Chau et. al. [2020] There are many applications for compliant mechanisms in Robotics, precision engineering, and bioengineering due to their low or non-existent friction, free lubrication, lack of backlash, single-piece construction, and ease of assembly. Unlike their rigid-body counterparts, compliant mechanisms' mechanical and kinematic characteristics are intrinsically linked, making design and analysis more challenging. Considering a multi-response optimisation strategy just compounds the difficulty of the problem. This research presents a unique effective hybrid approach to the multi-objective optimisation design of compliant systems. To demonstrate the effectiveness of the proposed optimisation strategy, we employ a bridge amplification mechanism with three numerical examples. This paper presents a hybridization of the desire function approach, the fuzzy logic system, the adaptive neuro-fuzzy inference system (ANFIS), the statistical methodology, and the finite element method for optimising the lightning attachment process. After constructing a 3D finite element model of the bridge amplification process, numerical tests are developed using a Box-Behnken layout. Fuzzy logic is then used to input the results, together with predictions for the mechanism's displacement and safety factor. This system's output is interpreted as a unified criterion. By constructing the ANFIS, the updated design variables are precisely matched with the FIS result. The LAPO method is then applied to the mechanism's multi-objective optimisation problem. Compared to Taguchi-based fuzzy logic, the findings favour the suggested approach. The proposed approach outperforms the Jaya algorithm and the TLBO algorithm using the Friedman test and the Wilcoxon signed rank test, respectively. The article's findings might be useful in trying times [12].

Alberto et. al. [2020] The optimisation of cable pressure distribution is seen in around 80% of the publications, with the primary objective being the attainment of an optimal design while minimising costs. In recent years, there has been a significant utilisation of optimisation algorithms across various domains. These applications encompass diverse areas such as the development of hybrid fibre reinforced polymeric deck and cables, the assessment of structural health, the analysis of existing bridges, and the implementation of passive and active control mechanisms to enhance dynamic performance [13].

Xia et. al. [2020] Model updating has shown to be an effective method for developing precise finite element models for bridge engineering designs. However, the effectiveness of existing optimisation methods decreases as the number of viable optimisation parameters increases. In order to improve the convergence process' efficiency and the likelihood of finding a global extremum, a combined model update strategy employing the response surface method and modified particle swarm optimisation (MPSO) was introduced. By simply modifying particle location with random Gaussian white noise, MPSO outperforms PSO in terms of test functions. Using a beam model update as an example, the convergence ability and accuracy of the suggested technique were compared to those of the genetic algorithm, which is often used to update bridge models. Finally, a model of an existing bridge with thirteen variables was successfully updated using the suggested approach [5].

Sabatino et. al. [2015] Highway bridges degrade during the course of their useful lives because of escalating traffic volumes and harsh environmental factors. The structural performance of highway bridges may be significantly impacted by the ageing of the materials. In order to analyse and eventually mitigate the negative

effects of structural collapse on the economy, society, and environment, a thorough risk assessment method is essential. The recommended framework for decision-support in maintenance optimisation offers life-cycle maintenance recommendations that effectively balance conflicting objectives, with a focus on sustainability. This paper uses utility theory to effectively assess the sustainability performance of highway bridges and examine the impact of decision makers' risk attitudes. The primary aim of this framework is to address and minimise the adverse consequences of structural collapse on the natural environment, societal well-being, and economic stability. On an existing highway bridge, the suggested approach's capabilities are shown [14].

Leander et. al. [2020] High strength steel may potentially lower the quantity of steel needed in bridge construction, allowing for a more environmentally friendly building process. In this research, a hybrid bridge made of steel and concrete is proven to have been optimised. High strength steel was compared to standard steel in terms of weight, material cost, and environmental effect to see whether it may provide any of these advantages. With the exception of fatigue, the optimization procedure complied with the Eurocode and met the requirements for the ultimate and serviceability limit states. A further check on the results of the optimization was done to examine the impact of weariness. According to study, using high strength steel might significantly reduce weight, environmental impact, and material costs. The potential benefits of using higher-quality steels, however, completely vanished when the Eurocode-compliant fatigue certification was taken into consideration [15].

Thippeswamy et. al. [2018] Cable stayed bridges are the preferred option for longer spans, and it's crucial to examine their behaviour under static and vehicular stress. Therefore, it is crucial that the analysis findings are more satisfying and the cable stayed bridge modelling is more accurate. However, in the current work, two distinct kinds of structural models, namely Spine Model and Area Object Model, are employed for the analysis of cable stayed bridge. There are several ways to use a structural model. In order to evaluate the outcomes, static analysis and moving vehicle analysis have been carried out with the application of the IRC Class A vehicle load. To choose the appropriate structural model for analysis, the analysis is carried out in CSi Bridge, and the analysis findings are evaluated using tables and graphs [16].

Wang et. al. [2021] Counterweights are usually meant to cooperate with cable pretension pressures in cable-stayed bridges to achieve a desirable final condition, particularly in asymmetrical bridges. To address the optimisation problem of the cable-stayed bridge, the integrated optimisation method (IOM) is developed to estimate cable forces and counterweights. The anchor points are suggested to be used in this manner by the counterweights. The problem is thus seen as a multi-objective one, with the least weighted total bending energy and the counterweight summaries serving as the two objective functions. The Pareto solution set is then realised by using a dynamic weighted coefficient approach to tackle this issue. An easy numerical model developed by IOM describes precise processes that are subsequently used to analyse the Yong-ding special-shaped cable-stayed bridge. The results show that by taking into account the counterweight dimension, IOM is able to not only realise the priority selection of the counterweight loading location but also to arrive at a more logical end state. Using the dynamic weighted coefficient method, decision-makers may quickly find the Pareto optimal solution set and then filter the results. Torsion and other spatial effects may be greatly

mitigated in cable-stayed bridges by using counterweights. It is possible to use IOM as a generic method of optimising cable-stayed bridges [17].

Huang et. al. [2018] The research on routing issues related to activities involving bridge inspection is presented in this article. An inspection team for bridges must depart from the depot with the faults identified, visit the bridges, and then come back to the depot. This task may take a single inspection team several days to accomplish, therefore the inspectors will need to make travel and lodging arrangements for the length of the inspection. This issue raises a unique category of vehicle routing issues (VRP). For the bridge inspection issue, there are two different sorts of situations developed. Only one inspection team is analysed in the first case, whereas several teams and a particular inspection period are evaluated in the second. The aim of this research is to identify the most cost-effective travel and hotel options, as well as the best routes for the inspection. An approach known as ant colony optimization (ACO) is used to tackle the issue. A local search technique is also suggested to raise the calibre of the solutions. To evaluate the performance of the suggested strategy, three benchmark datasets are created. The suggested technique is then applied to the benchmarks after selecting a set of ACO parameter values that produced overall positive results. The outcomes show that the suggested procedure produces promising results in a fair amount of time [18].

Shabanlou et. al. [2021] This research endeavour represents the first use of a flawless hybrid approach in the prediction of the scour pattern around a pair of bridge piers. The hybrid method, known as ANFIS-FA, is formed by integrating the "Adaptive Neuro-Fuzzy Inference System" (ANFIS) with the Firefly technique. The inclusion of the scour depth at twin piers and its influencing characteristics was subsequently included into the four ANFIS and ANFIS-FA models. The soft computing models were evaluated using Monte Carlo simulations. The k-fold cross validation method was also used to verify the accuracy of the numerical models. It's important to keep in mind that in k-fold cross validation, k = 5. According to the results of the research, ANFIS-FA models are more precise than ANFIS models. After a sensitivity analysis was built, the superior model could be identified. The superior model is affected by all input factors. This model does a decent job of predicting future scour levels. For instance, the R2, MAPE, and RMSE values were found to be 0.991, 5.876 and 0.015, respectively. More over two-thirds (66%) of the better model's outputs were within 5% of the true value, as determined by the error distribution findings. The Froude number (Fr) was ultimately determined to be the best input variable for predicting the scour hole around a pair of bridge piers. Based on the findings, it is evident that the performance of the ANFIS network may be enhanced by the use of the firefly technique. Furthermore, the performance of the hybrid model, ANFIS-FA, surpasses that of the original model. Ultimately, a thorough examination of uncertainty was conducted in order to reach the conclusion that the purported performance of the better model is, in fact, overstated. The results of the uncertainty analysis indicated that the hybrid model exhibited a narrower uncertainty band in comparison to the ANFIS model [19].

Hemant et. al. [2021] To horizontally cross a road, body of water, or valley is the primary function of a bridge. The design of a bridge may vary in accordance with its function and the characteristics of its immediate setting. For the bridge building to be completed successfully, the kind of bridge and the construction technique must

be carefully chosen while keeping in mind the bridge site and numerous limitations. Hilly terrain presents a special challenge for bridge building. It has been noted, nonetheless, that crucial obstacles in bridge building need to be recognised and assessed. The offered study work's primary goal is to identify crucial roadblocks to bridge building. The current evaluation study uses the newly created Multi Criteria Decision Making approach known as the "Best Worst Method" to calculate the relative weight age of the crucial obstacles in bridge building. There are a total of six major obstacles to building bridges. The essential obstacles in bridge building have also been rated using the Best Worst Method. A web-based poll of thirty stakeholder people provided the input data. The outcome will be crucial for the strategists in establishing effective strategies and methods to deal with significant obstacles in bridge building[20].

Wang et. al. [2022] After the bridge is built, the bridge's structural components will age and degrade due to environmental factors including weather and temperature. Static and dynamic stresses unavoidably weaken the rigidity and strength of bridge structures, such as the bridge deck and the bridge support. Understanding the modal features of a bridge is essential to dynamically identifying its structure and laying the groundwork for health monitoring. This study recommends a Bayesian approach to determining the modal parameters of bridges. Taking into consideration parameter uncertainty and the choice of modal parameters, the model is able to detect more local information thanks to the probability distribution of the parameters and a posteriori confidence. The Bayesian dynamic model monitors the bridge's dependability in real time, and since the monitoring error is so low (0.01), it is possible to identify the bridge's modal parameters with great accuracy[21].

Saman et. al. [2023] Bridges play a significant role in civil engineering and are essential components of the infrastructure. Monitoring the health of a bridge is essential for maintaining its safety and extending its lifespan. The structural stability of these structures is extended and greatly helped by routine monitoring. Based on various theories and laboratory testing, many researchers have suggested various techniques for determining bridge damages. Several literature reviews on the topic of fracture and damage detection in bridges have been produced during the last several decades. In this study, a number of methods and theoretical frameworks for detecting deterioration in bridge designs are examined. The purpose of this essay is to assess several approaches that have been put out to find deterioration in various bridges critically. Several articles have undergone comprehensive scrutiny, and the shortcomings and superiority of the methodologies used have been noted. Future applications and a number of sustainable techniques that are important for bridge monitoring are also discussed in the majority of assessments. This work makes important contributions to the existing body of knowledge by critically examining existing methods, recommending methods that may more accurately identify damage to bridge structures, and serving as a helpful reference for future research[22].

Mohandas et. al. [2020] A bridge is a structure that enables transportation to pass over an impediment without obstructing the road below. A pipeline, a canal, a road, a train, or pedestrians may all need a route. These days, bridge deck portions in the shape of boxes are often used. Most bridges are constructed using box girders. Today, post-tensioning is a technique that is widely used in bridge building. Most bridges are of the prestressed

kind (mostly post-tensioned). In this paper, an effort is made to conduct comparative research of several prestressed bridge types by altering the bridge's various properties[23].

K. Senthil et. al. [2017] Three-dimensional numerical analyses completed on railroad bridges are used to organise the usage of Abaqus / Explicit finite detail implementation. The present study will take into account a single vehicle and a bridge that is 30 metres long. The JC version to be employed in ABAQUS had been used to predict the constitutive and fracture behaviour of medicines. Participants in the bridge test must have access to all materials specified in the JC template. Bridge solutions were anticipated given the strain and von-misses. The inspections were performed taking into mind the aesthetic value and AA loading of the bridge. By altering the intensity as 1600, 1400, 1200, and 1000 mm, the effect of primary girder intensity was evaluated. By splitting the span of the bridge in two and taking that into consideration as a strengthening strategy, the reactions of bridges are evaluated. The behaviour of the bridges was further studied by eliminating the midspan cross girders under the assumption of member failure or corrosion[24].

Alpesh et. al. [2016] This analysis describes an experimental assessment of the structural behaviour of a glass fibre reinforced polymer (GFRP) area truss bridge subjected to static stress. The prototype bridge was constructed using bolts made of metal, GFRP brackets and profiles manufactured by Fibre Line Composites Ltd. To facilitate loading, a wooden bridge deck was installed. The bridge node displacement was monitored while subjecting it to a total applied force of 13.3 kilonewtons (KN) over four different ranges. The truss form's flexural response was consistently evaluated throughout the loading process. Comparative analysis demonstrates that the experimental and numerical findings are in good accord. According to the findings, there was an adequate supply of structural stiffness in the bridge model that was developed and evaluated. The findings of a reputable research support the viability of using GFRP profiles as the actual bridge superstructures for pedestrian bridges[25].

Z. Zheng et. al. [2017] They studied the possibility of a slow building collapse. If the third side pillar is under impact load, more severe damage will occur, and if the pillar falls after the accident, progressive collapse will occur, as shown by the results for the load examples below. A finite element truss model consisting of six trusses was developed for this study using ANSYS/LS-DYNA dynamic analysis software. It reenacts real-life collisions between huge vehicles and structures. The study demonstrated that truss systems exhibit varying degrees of stress and strain, which are contingent upon factors such as the severity of the impact load, the location of the crash site, and the ratio of structural height to span. The possibility of a gradual collapse of the structure, as opposed to only the failure of individual parts, was investigated in this paper[26].

Emdadul Hoque et. al. [2017] examined the mechanical behaviour of a steel truss bridge model using a simple support system. For the simulations and geometric modelling, they employed ANSYS Workbench 15.0. The harmonic response of the bridge was found by applying a 100N excitation sinusoidal force uniformly distributed across its deck with an analytical frequency range of 0-1000Hz. Modal analysis was used to determine the natural frequencies for the first fifteen modes. The interactions between the bridge and the load are visually and analytically represented in terms of total deformations and equivalent stresses taking frequency variation into account. The combination of analytical and visual outcomes provides a complete

approach to geometric optimisation in order to prevent resonance in the steel truss bridge model. This optimisation process has the potential to be used in the construction of an actual steel truss bridge. They all take into account the potential for various degrees of vibrations[27].

Huili Wang et. al. [2017] The steel truss integral joint's multi-scale FEM is used to calculate the fatigue efficiency. Numerical results are verified for experimental results. The setting of the evaluation of the fatigue effectiveness of the steel belt integrated joint is a crossing of a suspension bridge. The connection components are used in both the beam and three-dimensional structures. The relation aspect consists of two joints, one of which has six degrees of freedom. These degrees of freedom are divided into three degrees of translation and three degrees of rotation. When all six degrees of freedom are considered together, they contribute to the overall functionality of the joint. The outcomes of the tests conducted using the multi-scale finite element method FEM) exhibit a high degree of similarity to those obtained by experimental means. The primary testing component may be precisely quantified, and a prediction of the fatigue life can be made, simplifying the multi-scale FEM. It is a highly practical and successful approach. An innovative and efficient approach of structural analysis fatigue efficiency is provided by multi-scale FEM[28].

Jayakrishnan. T J et. al. [2017] The study of seismic bridge behaviour with ANSYS software has been examined. Composite structures have several practical uses in the fields of architecture, civil infrastructure, and aircraft. Spectrum response system is used to examine the seismic behaviour of composite bridges. The shape, material, setup, chosen response spectrum, and details of device assembly all affect how the structure reacts. The ANSYS Workbench finite element tool is used in this research to examine the seismic behaviour of composite bridges[29].

CHAPTER- 3

RESEARCH GAP AND OBJECTIVES

3.1 Problem Identification

The presence of cracks on bridges tends to cause disruption in natural frequency. Any change in natural frequency can vary the dynamic characteristics of bridge which in turn can cause amplitude build up and ultimately failure of bridge structures. The thorough investigation of induced crack on bridge structures is vital for evaluating the structural stability of the bridge.

3.2 Objectives

The primary aim of the present study is to assess the impact of crack dimensions on the vibration characteristics of bridges. The analysis is conducted using ANSYS FEA simulation package.

1. CAD modelling and FEA simulation of bridge structure generic design to determine natural frequency and mode shapes.
2. CAD modelling and FEA simulation of bridge structure with crack to determine natural frequency and mode shapes.
3. Evaluating the effect of crack dimensions on bridge vibration characteristics using RSM technique.

CHAPTER- 4

METHODOLOGY

4.1   Methodology Flow Chart

```
        Need of research
               │
               ▼
      Problem identification
               │
               ▼
       Literature review
               │
               ▼
  CAD modelling of steel I girder bridge
               │
               ▼
  Modal analysis of base design using ANSYS software
               │
               ▼
  Modal analysis of bridge design with cracks using ANSYS software
               │
               ▼
  Selection of optimization variables and conducting RSO
               │
               ▼
  Comparison of dynamic characteristics for both generic design and crack induced design
               │
               ▼
         Conclusion
```

4.2   Material Definition

Establishing a precise definition of the material in question is the first stage of the procedure. The geometry under consideration incorporates both concrete and structural steel. Figure 4.1 depicts the material characteristics of structural steel[30].

	Properties of Outline Row 5: Structural Steel				▾ ⊓ ✕
	A	**B**	**C**	**D**	**E**
1	Property	Value	Unit	⊗	↩
2	Material Field Variables	Table			
3	Density	7850	kg m^-3 ▾	□	□
4	⊟ Isotropic Secant Coefficient of Thermal Expansion			□	
5	Coefficient of Thermal Expansion	1.2E-05	C^-1 ▾		□
6	⊟ Isotropic Elasticity			□	
7	Derive from	Young'... ▾			
8	Young's Modulus	2E+11	Pa ▾		□
9	Poisson's Ratio	0.3			□
10	Bulk Modulus	1.6667E+11	Pa		□
11	Shear Modulus	7.6923E+10	Pa		□

Figure 4.1: Material property definition of steel [30]

Figure 4.2 depicts the ANSYS material definition window for the bridge deck's concrete material. The material properties of concrete are derived from the literature[31].

	A	B	C	D	E
1	Property	Value	Unit	⊗	↻
2	📊 Material Field Variables	📋 Table			
3	📊 Density	2448	kg m^-3 ▾	☐	☐
4	⊟ 📊 Isotropic Elasticity			☐	
5	Derive from	Young'... ▾			
6	Young's Modulus	28000	MPa ▾		☐
7	Poisson's Ratio	0.2			☐
8	Bulk Modulus	1.5556E+10	Pa		☐
9	Shear Modulus	1.1667E+10	Pa		☐

Properties of Outline Row 4: concrete paper

Figure 4.2: Material property definition of concrete [31]

4.3   Bridge Structure Designing

The design of the bridge is created using the design modeller framework of the ANSYS software. Initially, "I"-shaped girders are fabricated using the bridge framework. The ANSYS Design Modeller establishes the variable dimensions. H1 and V2 are the critical dimensions, as depicted in Figure 4.3. H1 represents the beam's horizontal dimension, while V2 represents its vertical dimension.
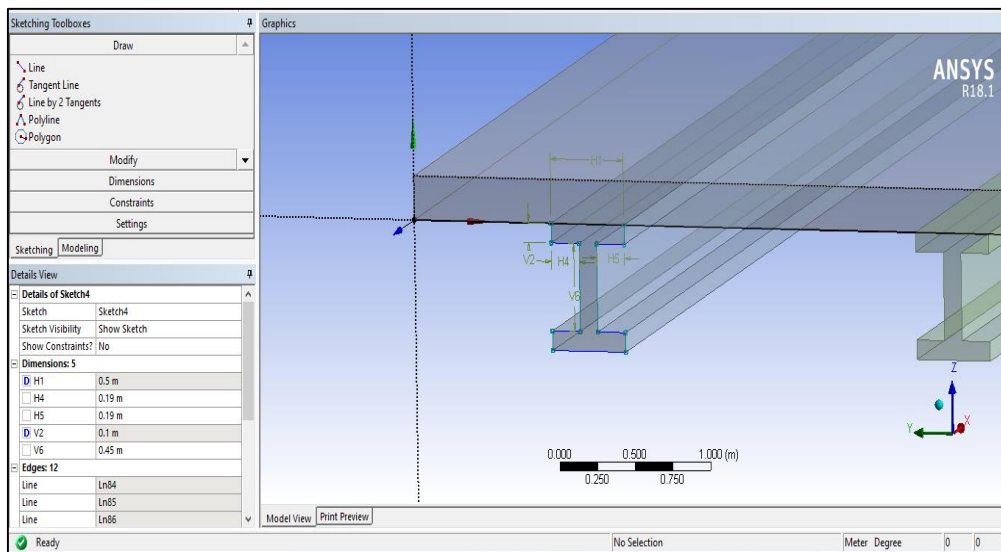
Figure 4.3: Variable selection in ANSYS design modeller

Name	Value	Type
✓ girder_width	0.5 m	Length
✓ flange_thickness	0.1 m	Length

Figure 4.4: Definition and assigning of optimization variables

Figure 4.5 shows the process of constructing the bridge deck after I-shaped girders have been simulated. The bridge deck is built using sketching and extruding tools and then bolted to I-shaped girders.
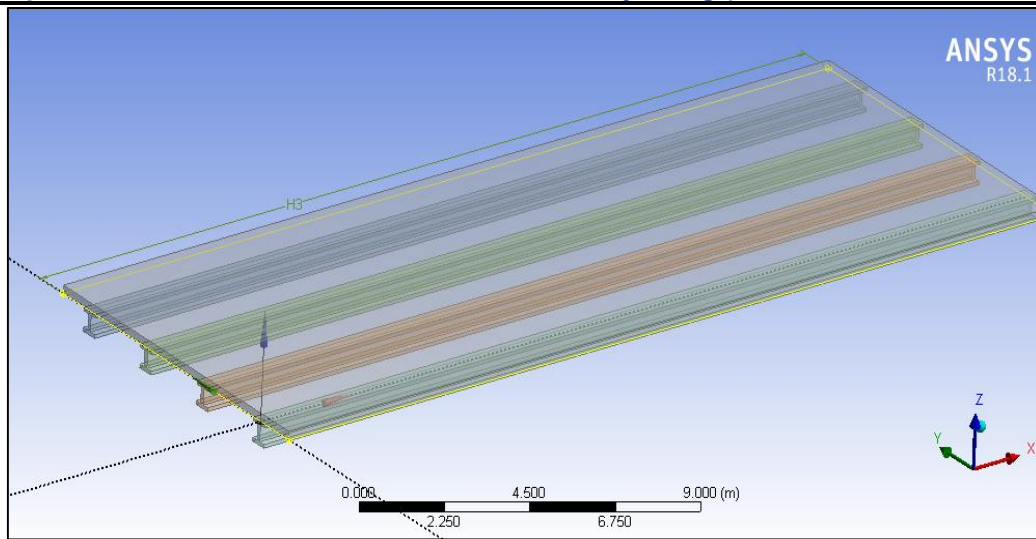
Figure 4.5: Bridge deck model and I shaped girder

4.4   Meshing

Build a mesh for the model using brick elements. Each component made of bricks has three degrees of freedom (DOFs) and is made up of eight nodes. Figure 4.6 is a picture of a part that looks like a brick, which is a rectangular block that is usually made of stone or clay. The rate of change has been determined to be fast, and the sizes of the parts have been deemed to be moderate. At 0.272, both the transition ratio and the most layers that can be in the inflation setup have been set. The finished product has 2910 different parts and 17922 different points of connection. The mesh model is shown in Figure 4.6.
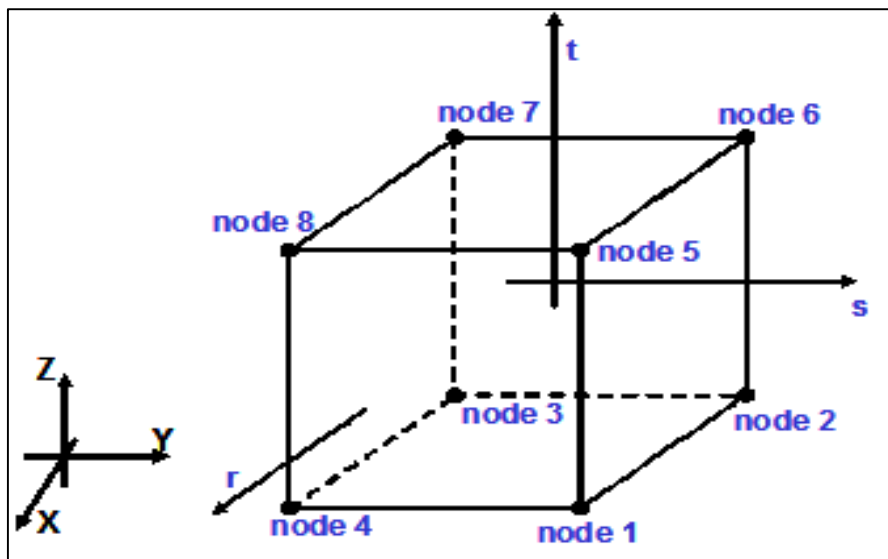
Figure 4.6: Element shape of hexahedral/brick type element
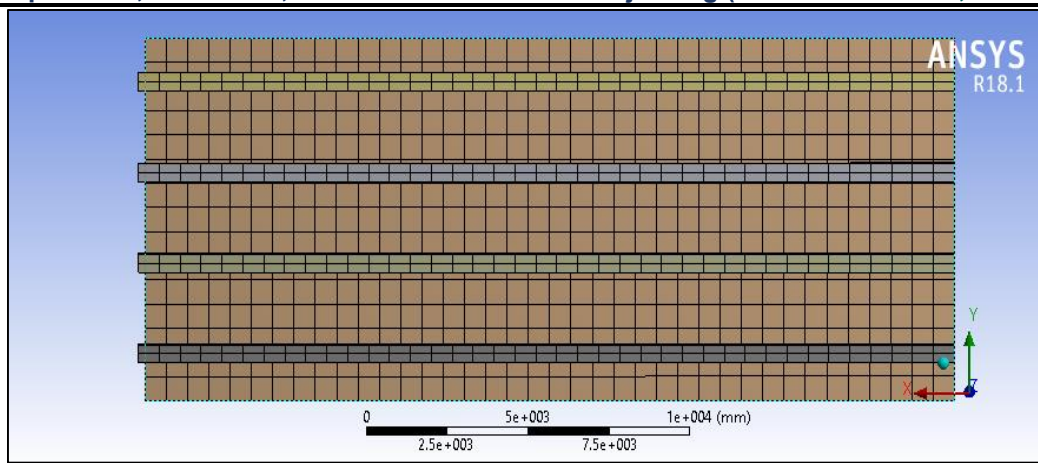
Figure 4.7: Meshed model of bridge structure

4.5 Structural Boundary Conditions

Once the process of discretization is completed, the structural boundary conditions are then applied to the bridge model. The displacement type structural support, with three degrees of freedom fixed, is applied to each end faces of the bridge. The displacement type support is designed to limit movement in the x, y, and z axes.
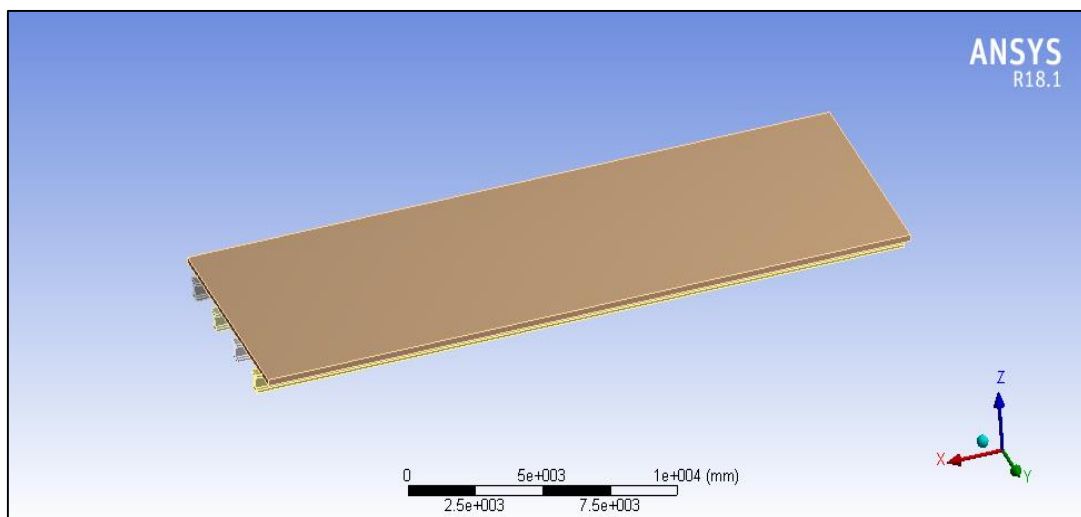
Figure 4.8: Applied structural boundary conditions

4.6   Modelling of Crack

In the subsequent phase, the crack is initiated on the girder. The model used in this study represents a crack of the "elliptical" type. Figure 4.9 depicts the girder exhibiting a crack.
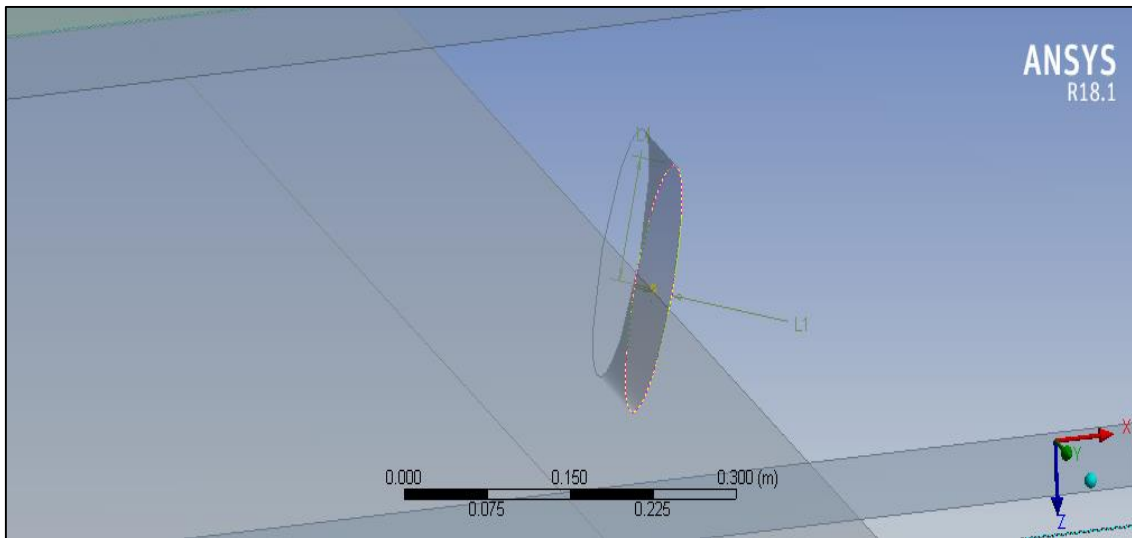
Figure 4.9: Girder with elliptical crack

Two variables, L1 and L4, are defined to represent cracks, specifically a minor crack and a major crack. The dimensions have been chosen (see Figure 4.10). The length of L1 measures 0.018 metres, while the length of L4 measures 0.09 metres.
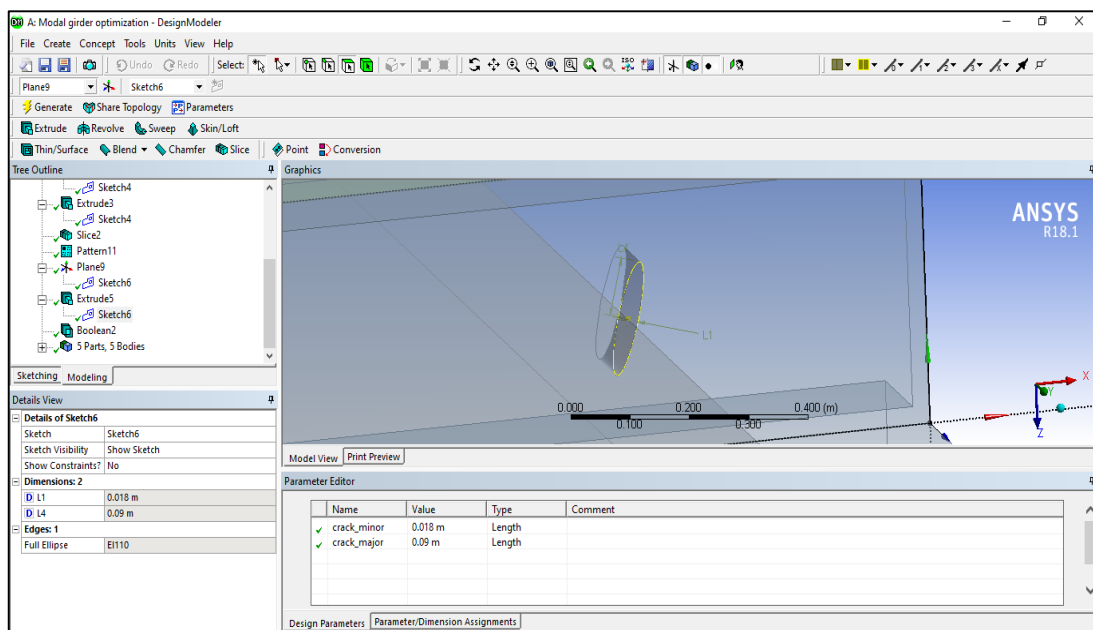
Figure 4.10: Dimensional variable definition

4.7   Response Surface Optimization

The term "response surface method" (RSM) refers to a collection of mathematical and statistical methods used to analyse issues when a number of independent factors have an impact on a dependent variable or response[32]. The primary objective is to elicit a more favourable response. The proposition is made that these elements exhibit a condition of enduring nature, in which the researcher possesses the ability to make alterations to them, and they can be distinguished from X1, X2, X3, X4, and subsequent elements [33]. The equation Y = f(X1, X2, X3, X4,......, Xn) can be utilised to illustrate the correlation between the dependent

variable and the independent variables. This equation seeks to determine the source or origin of the noise or error present in the "y" solution.

The mathematical representation f(X1, X2, X3, X4,...... Xn) = Y is commonly referred to as the response surface, under the condition that the anticipated outcome E(y) = f(X1, X2, X3, X4,...... Xn) [46]. The image and accompanying data presented depict the selected input values that were chosen to enhance the subject matter at hand.

CHAPTER- 5

RESULTS AND DISCUSSION

5.1 Bridge Without Crack (Generic Design) Results

The vibration characteristics of a generic design (specifically, a bridge without any cracks) are assessed through modal analysis. The mode shapes are determined for every individual frequency.
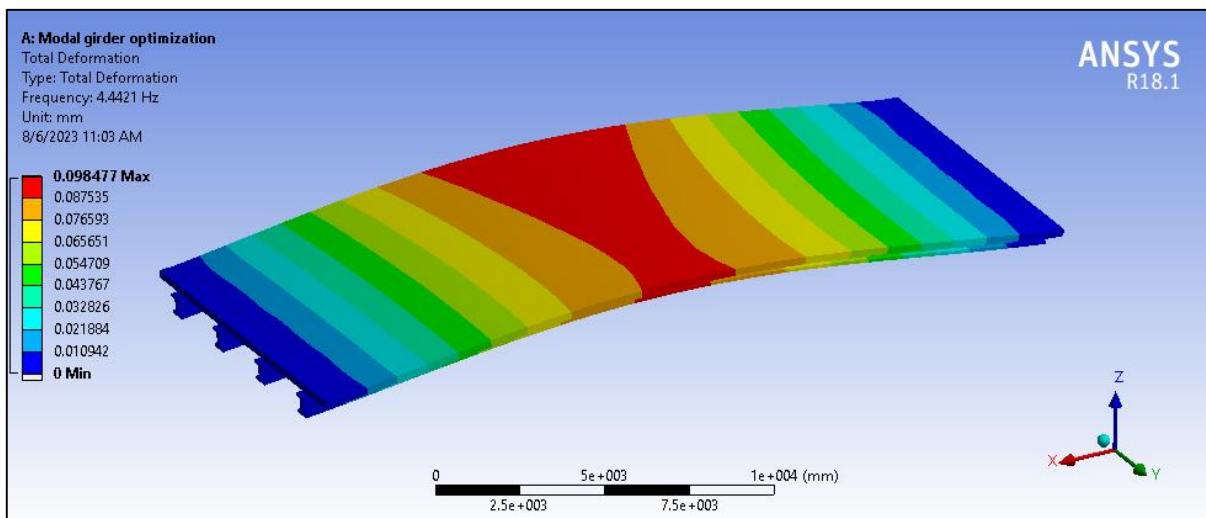
Figure 5.1: 1st mode shape of generic design

Based on the conducted modal analysis, the first natural frequency obtained is determined to be 4.4Hz, indicating a transverse mode. The maximum deformation achieved from the first mode shape is 0.098mm.
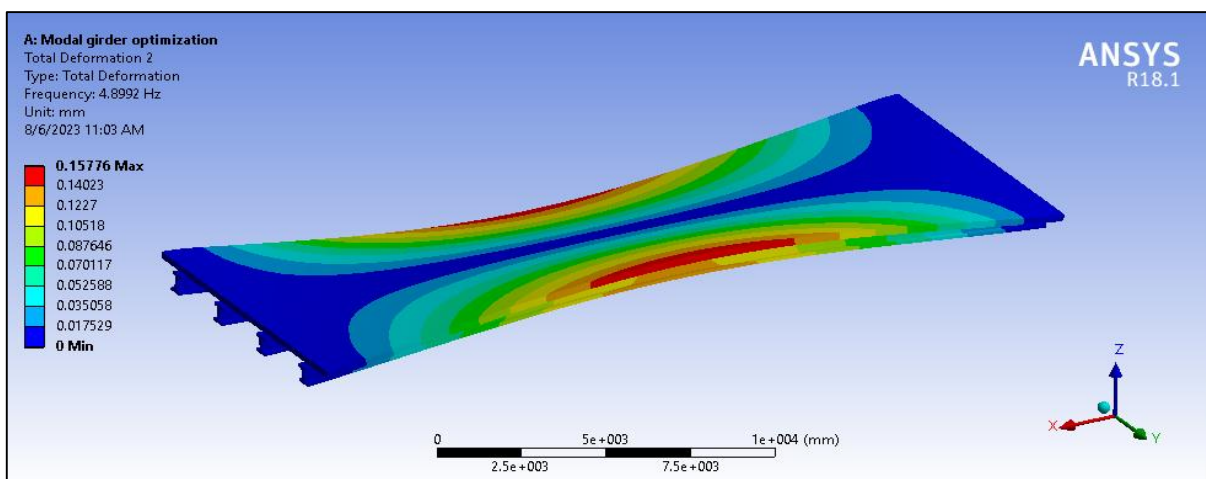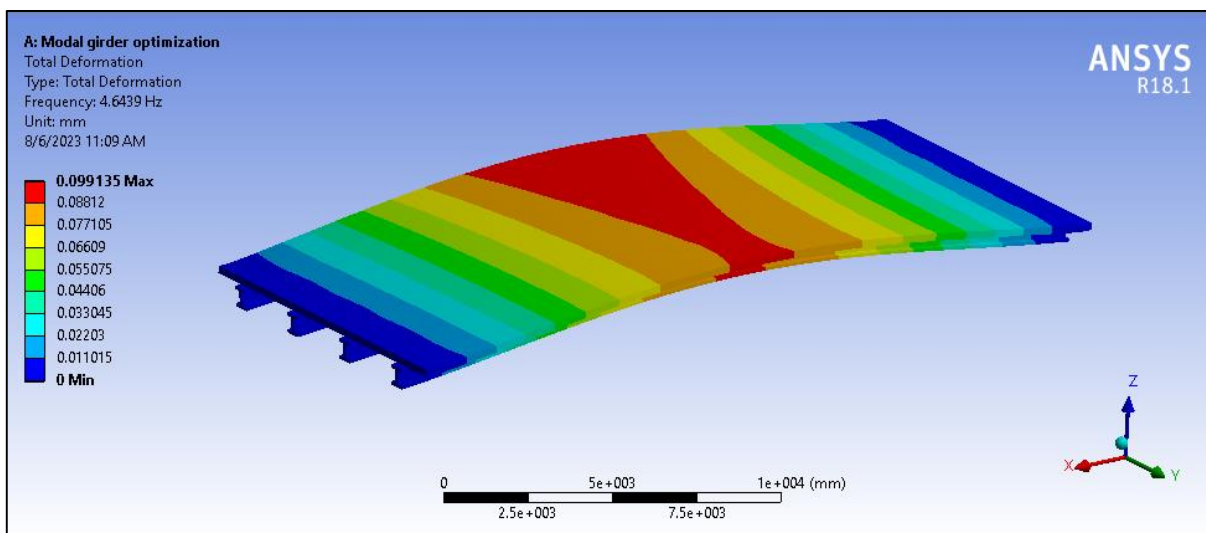

Figure 5.2: 2nd mode shape of generic design

Based on the conducted modal analysis, the second natural frequency obtained is determined to be 4.8Hz, indicating its classification as a transverse type. The maximum deformation achieved from the second mode shape is 0.157mm.
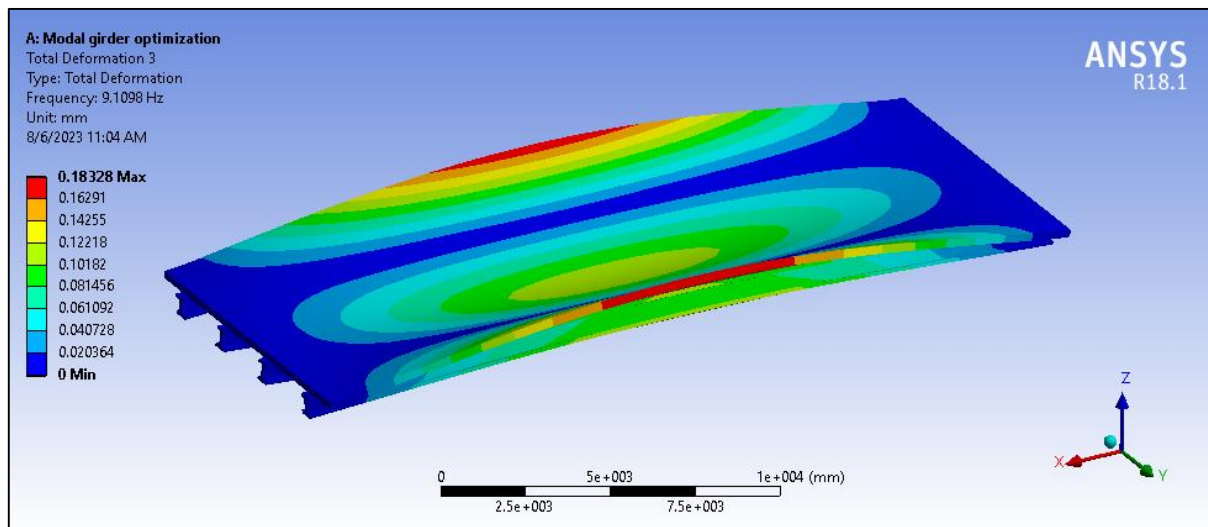
Figure 5.3: 3rd mode shape of generic design

The third natural frequency is determined for a generic design, as shown in Figure 5.3. The observed natural frequency is measured to be 9.1098 Hz, while the corresponding maximum deformation is approximately 0.162 mm. The deformation of the side edges of the bridge structure is greater in comparison to the mid zone.
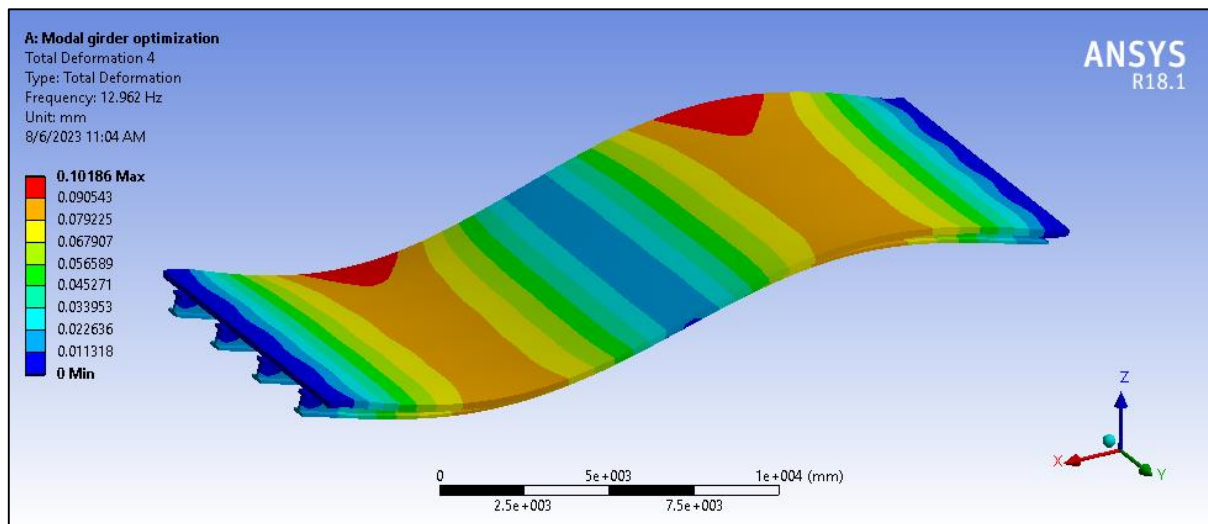
Figure 5.4: 4th mode shape of generic design

The 4th natural frequency is acquired for a generic design, as depicted in Figure 5.4. The observed natural frequency is measured to be 12.962 Hz, while the corresponding maximum deformation is approximately 0.1018 mm. The deformation of the side edges of the bridge structure is greater in comparison to the mid zone. The vibrational characteristics are of the "transverse" type.
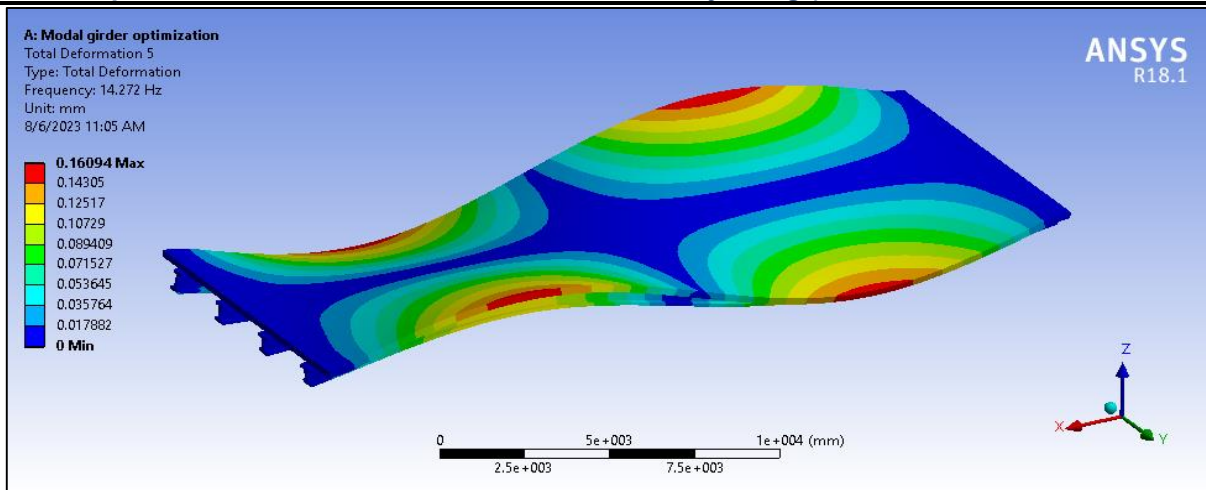
Figure 5.5: 5th mode shape of generic design

The 5th natural frequency for the generic design is obtained through the conducted modal analysis, as shown in Figure 5.5. The observed natural frequency is measured to be 14.272 Hz, while the corresponding maximum deformation is approximately 0.14305 mm. The deformation of the side edges of the bridge structure is greater in comparison to the mid zone. The vibrational characteristics exhibit a "torsional" nature.

5.2   Bridge with Crack Results

The natural frequencies and mode shapes of a bridge deck with a crack are determined. The mode shapes are determined for every individual frequency. Based on the conducted modal analysis, the first natural frequency observed is 4.6Hz, indicating a transverse mode. The maximum deformation achieved from the first mode shape is 0.099mm.

Figure 5.6: 1st mode shape of cracked geometry

Based on the conducted modal analysis, the second natural frequency obtained is determined to be 5.09Hz, indicating its classification as a torsional mode. The maximum deformation resulting from the second mode shape is measured to be 0.1586 millimetres.
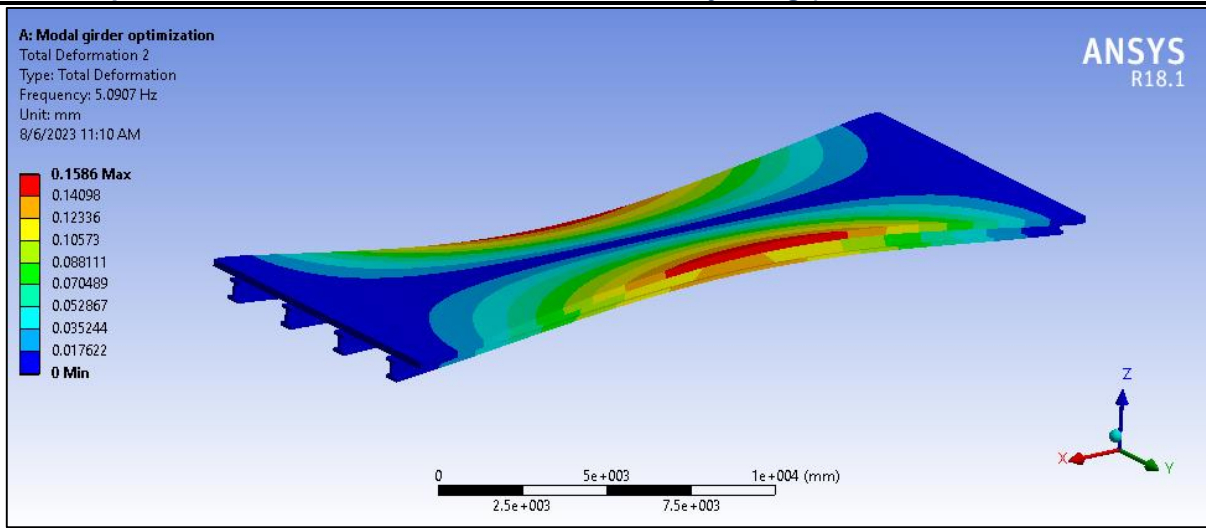
Figure 5.7: 2nd mode shape of cracked geometry

The third natural frequency is determined for the cracked design geometry, as shown in Figure 5.8, based on the conducted modal analysis. The observed natural frequency is 9.2 Hz, and the corresponding maximum deformation is approximately 0.1635 mm. The deformation of the side edges of the bridge structure is greater in comparison to the mid zone. The vibrational characteristics exhibit a "torsional" nature.
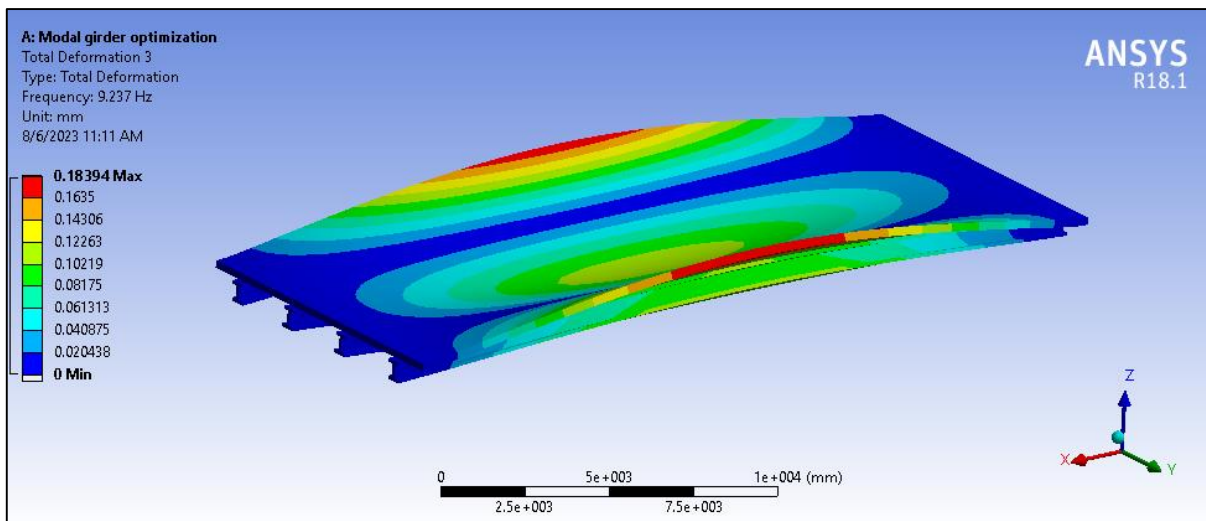
Figure 5.8: 3rd mode shape of cracked geometry

The 4th natural frequency is determined for the cracked design geometry based on the conducted modal analysis (see figure 5.9). The observed natural frequency is measured to be 13.32 Hz, while the corresponding maximum deformation is approximately 0.0909 mm. The deformation of the side edges of the bridge structure is greater in comparison to the mid zone. The vibrational characteristics are of the "transverse" type.
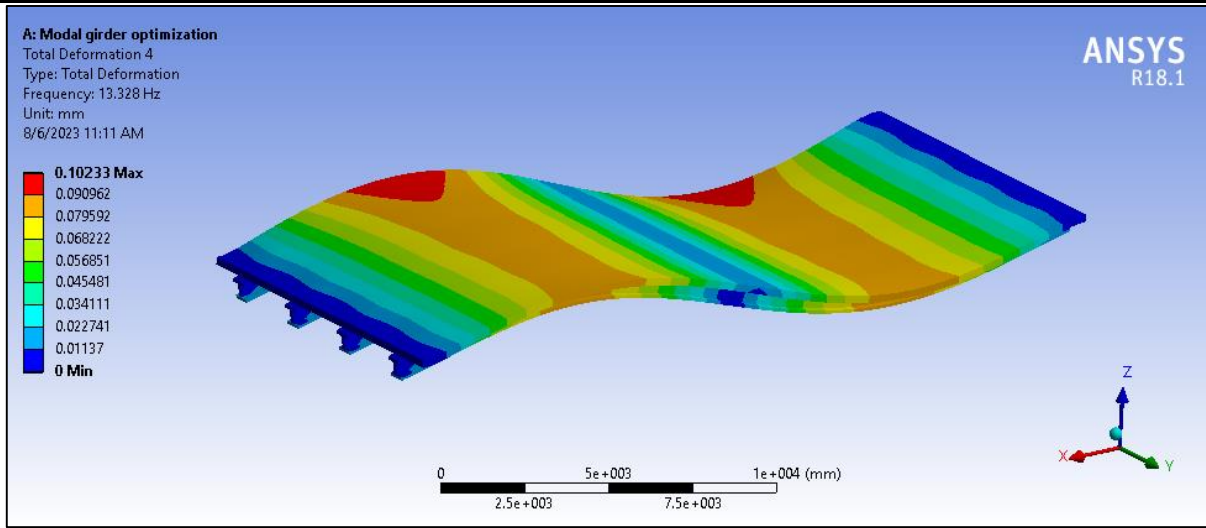
Figure 5.9: 4th mode shape of cracked geometry

The 5th natural frequency is determined for the cracked design geometry (as shown in Figure 5.10) based on the conducted modal analysis. The observed natural frequency is 14.488 Hz, and the corresponding maximum deformation is approximately 0.1427 mm. The deformation of the side edges of the bridge structure is greater in comparison to the mid zone. The vibrational characteristics are of the "torsional" type.
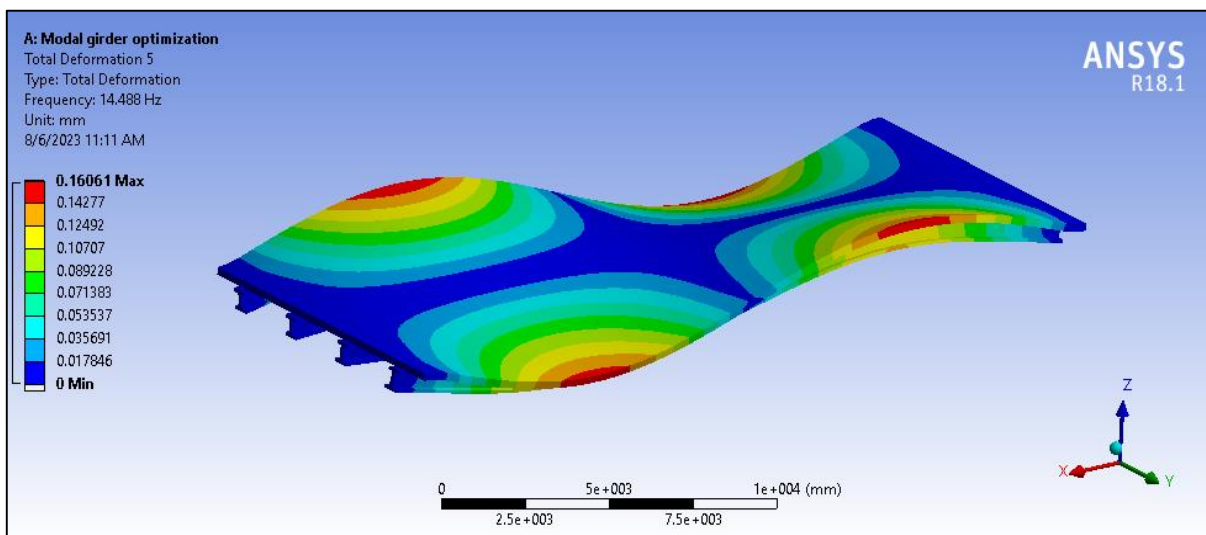
Figure 5.10: 5th mode shape of cracked geometry

Table 5.1: Natural frequency comparison table

Design Type	1st natural frequency	2nd natural frequency	3rd natural frequency	4th natural frequency	5th natural frequency
Without crack	4.4421	4.8992	9.1098	12.962	14.272
With crack	4.6439	5.0907	9.237	13.328	14.488

Natural Frequency comparison
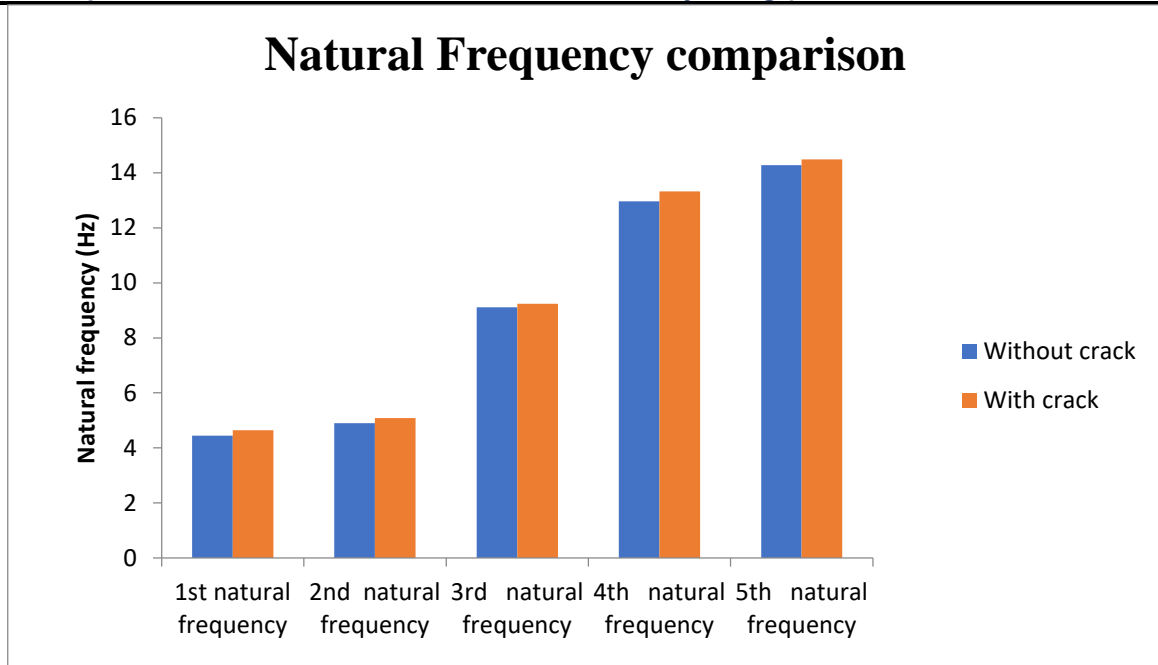
Figure 5.11: Natural frequency comparison

According to the natural frequency comparison chart depicted in Figure 5.11 above, it can be observed that the bridge without any cracks exhibits lower natural frequencies in comparison to the bridge with cracks.

Table 5.2: Natural frequency deformation table

Design Type	1st natural frequency	2nd natural frequency	3rd natural frequency	4th natural frequency	5th natural frequency
Without crack	.0984	.157	.183	.1018	.1609
With crack	.0991	.1586	.18394	.10233	.16061
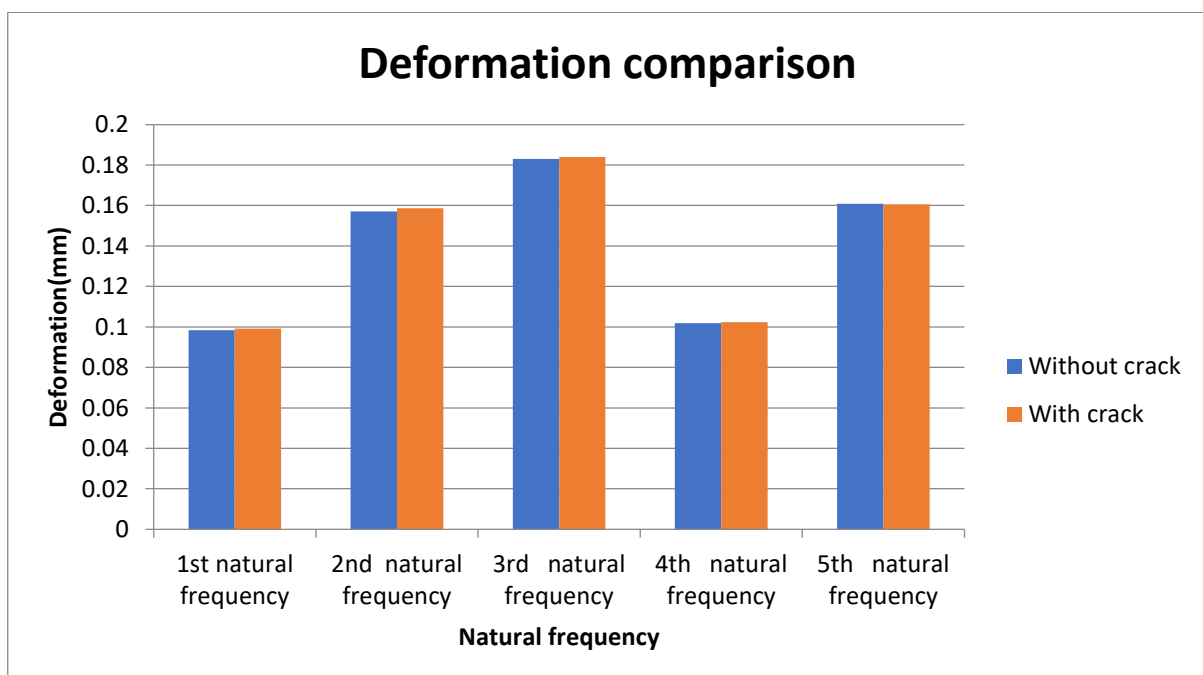
Figure 5.12: Natural frequency deformation comparison

The first four natural frequencies of the bridge exhibit higher deformation in the presence of a crack, while lower deformation is observed in the absence of a crack. In the case of the fifth natural frequency, it can be observed that the bridge without a crack exhibits greater deformation in comparison to the bridge that does possess a crack. In the case of beams with equal spans, the modes exhibit either a symmetric or antisymmetric configuration, and these modes are mutually exclusive, enabling their separate analysis. This approach facilitates the establishment of a correlation between the fundamental frequency of multi-span bridges and that of single-span bridges. As stated in Equation (5.1), a fundamental span bridge with a span length denoted as L demonstrates a principal circular frequency equivalent to L, whereas its nth circular frequency is denoted as nL.

$$\omega_{sb} = \frac{(n\pi)^2}{(nL)^2} \sqrt{\frac{EI}{m}} \quad \ldots.(1)$$

5.3   Application of Response Surface Method (RSM)

Using the RSM technique, different design points are generated. In total 9 different design points are generated by varying "girder_width" and "flange_thickness" value as shown in figure 5.13. The 5 frequency values are obtained for each individual design points.

	A	B	C	D	E	F	G	H
1	Name	P1 - girder_width (m)	P2 - flange_thickness (m)	P3 - Total Deformation Maximum (mm)	P4 - Total Deformation 2 Maximum (mm)	P5 - Total Deform... 3 Maximum (mm)	P6 - Total Defor... 4 Maximum (mm)	P7 - Total Deforma... 5 Maximum (mm)
2	1 DP 0	0.5	0.1	0.098477	0.15776	0.18328	0.10186	0.16094
3	2	0.45	0.1	0.10769	0.16782	0.19328	0.11495	0.17205
4	3	0.55	0.1	0.091206	0.14947	0.1738	0.092422	0.14948
5	4	0.5	0.09	0.10022	0.16063	0.18645	0.104	0.16319
6	5	0.5	0.11	0.096983	0.15519	0.18023	0.099914	0.15889
7	6	0.45	0.09	0.10948	0.17086	0.1966	0.1175	0.17365
8	7	0.55	0.09	0.09273	0.15203	0.17685	0.094199	0.15192
9	8	0.45	0.11	0.10599	0.16493	0.19008	0.11252	0.17034
10	9	0.55	0.11	0.089722	0.14706	0.17088	0.090687	0.14727

Table of Outline A2: Design Points of Design of Experiments

Figure 5.13: DOE chart

The max. and min. values of individual frequencies are obtained from the overall DOE data generated as shown in figure 5.13 above. The max. and min. values obtained are shown in figure 5.14.

	A	B	C
1	Name	Calculated Minimum	Calculated Maximum
2	P3 - Total Deformation Maximum (mm)	0.089722	0.10948
3	P4 - Total Deformation 2 Maximum (mm)	0.14706	0.17087
4	P5 - Total Deformation 3 Maximum (mm)	0.17088	0.1966
5	P6 - Total Deformation 4 Maximum (mm)	0.090687	0.11751
6	P7 - Total Deformation 5 Maximum (mm)	0.14727	0.17365

Figure 5.14: Max. and min. values of first 5 frequencies

As per the findings of the analysis, the initial natural frequency exhibits a maximum deformation of 0.109mm and a minimum deformation of 0.08mm. In rows 2, 3, 4, and 5, the highest and minimum numbers of the second, third, fourth, and fifth frequency mode forms are also shown. The slope of the goodness-of-fit, as depicted in Figure 5.15, is obtained through the process of optimising the reaction surface. The predicted value is shown by a straight line, which comes from a linear regression model. The visual representation of distortion levels at various natural rates is depicted by coloured circles, which accurately indicate the observed values. A smaller degree of dispersion in the goodness of fit graph indicates a higher degree of proximity between the observed values (cells) and the predicted values (represented by the straight line), as evidenced by the shape of the goodness of fit curve.
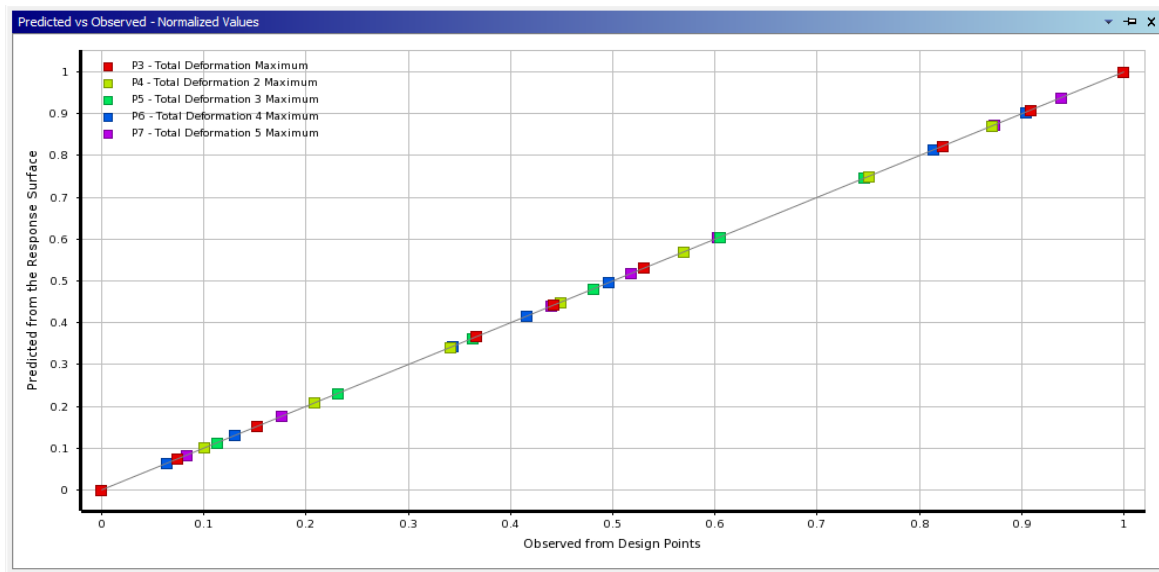
Figure 5.15: Statistical chart representing goodness of fit curve

The range of values are determined for total deformation obtained. From the RSM plot shown in figure 5.16, the max. values of deformation are represented in red color and min. values are represented in dark blue coloured region.

Table 5.3: RSM data of max. 1st frequency total deformation

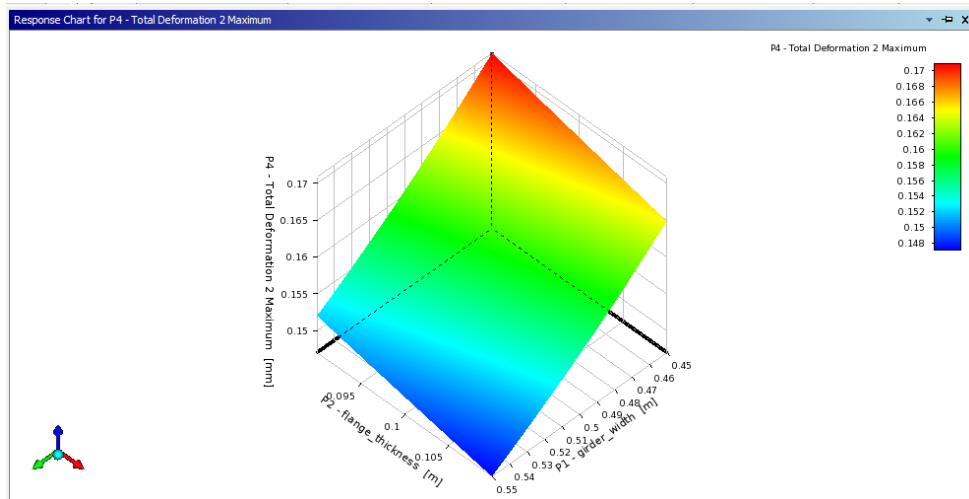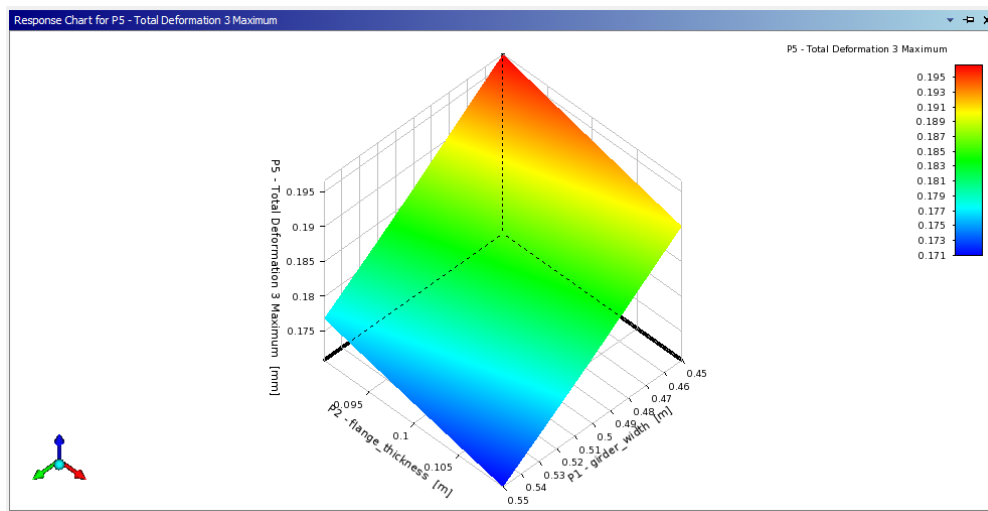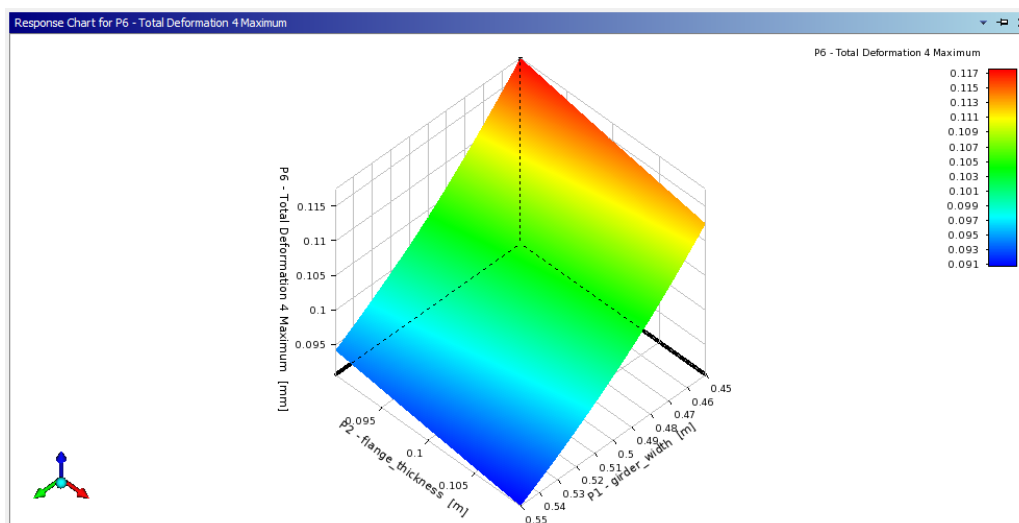| Flange Thickness Range	.090mm to .105mm
Girder Width Range	.45mm to .47mm
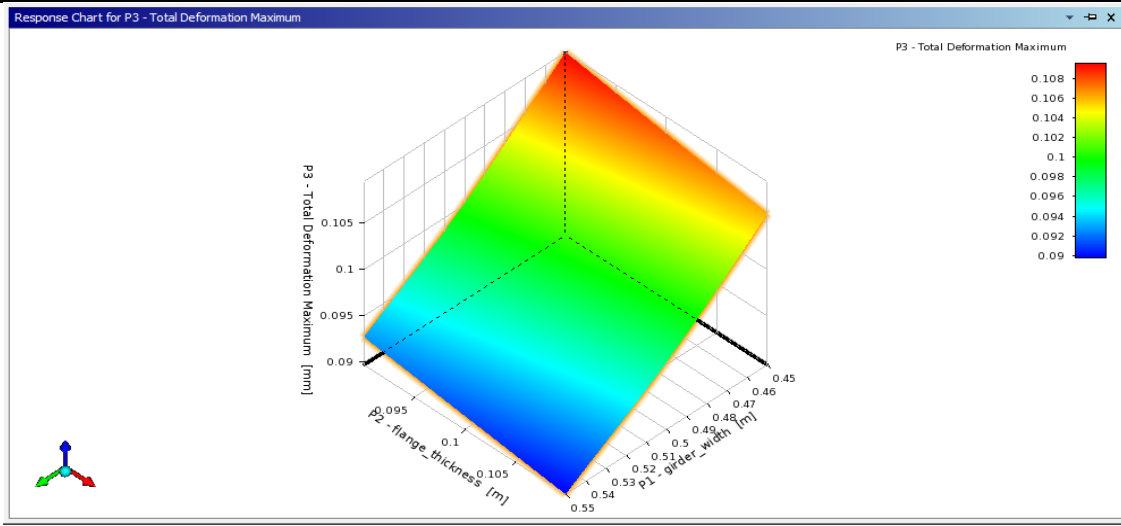
Figure 5.16: RSM plot of 1st frequency deformation

The range of values are determined for 2nd frequency deformation. From the RSM plot shown in figure 5.17, the max. values of deformation are represented in red color and min. values are represented in dark blue coloured region.

Table 5.4: RSM data of max. 2nd frequency total deformation

Flange Thickness Range	.090mm to .105mm
Girder Width Range	.45mm to .475mm

Figure 5.17: RSM plot of 2nd frequency deformation

The range of values are determined for 3rd frequency deformation. From the RSM plot shown in figure 5.18, the max. values of deformation are represented in red color and min. values are represented in dark blue coloured region.

Table 5.5: RSM data of max. 3rd frequency total deformation

Flange Thickness Range	.090mm to .105mm
Girder Width Range	.45mm to .48mm

Figure 5.18: RSM plot of 3rd frequency deformation

The range of values are determined for 4th frequency deformation. From the RSM plot shown in figure 5.19, the max. values of deformation are represented in red color and min. values are represented in dark blue coloured region.

Table 5.6: RSM data of max. 4th frequency total deformation

Flange Thickness Range	.091mm to .108mm
Girder Width Range	.45mm to .47mm

Figure 5.19: RSM plot of 4th frequency deformation

The range of values are determined for 5th frequency deformation. From the RSM plot shown in figure 5.20, the max. values of deformation are represented in red colour and min. values are represented in dark blue coloured region.

Table 5.7: RSM data of max. 5th frequency total deformation

Flange Thickness Range	.091mm to .109mm
Girder Width Range	.45mm to .48mm
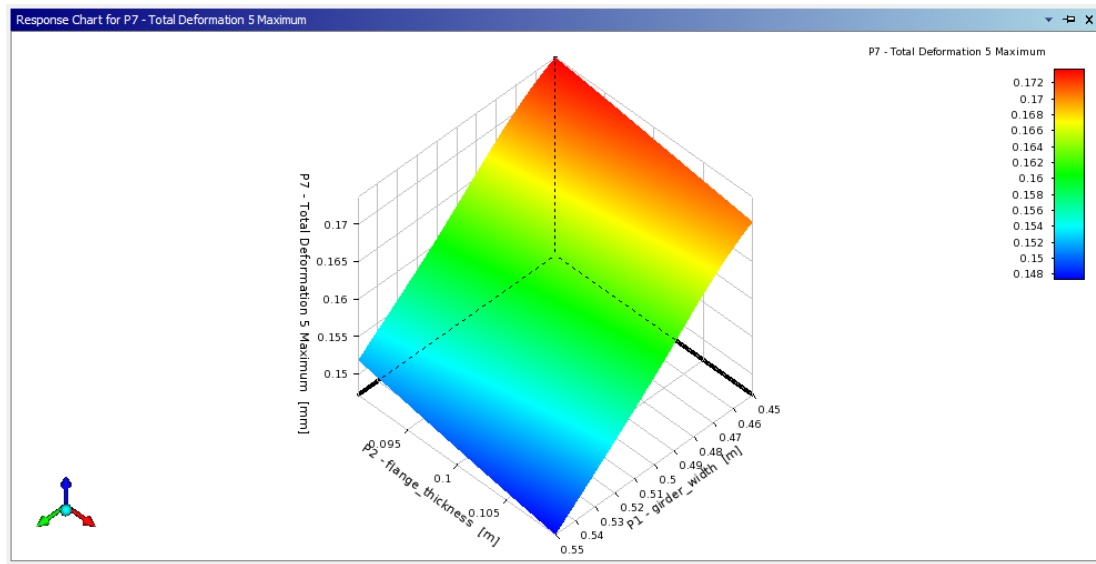
Figure 5.20: RSM plot of 5th frequency deformation
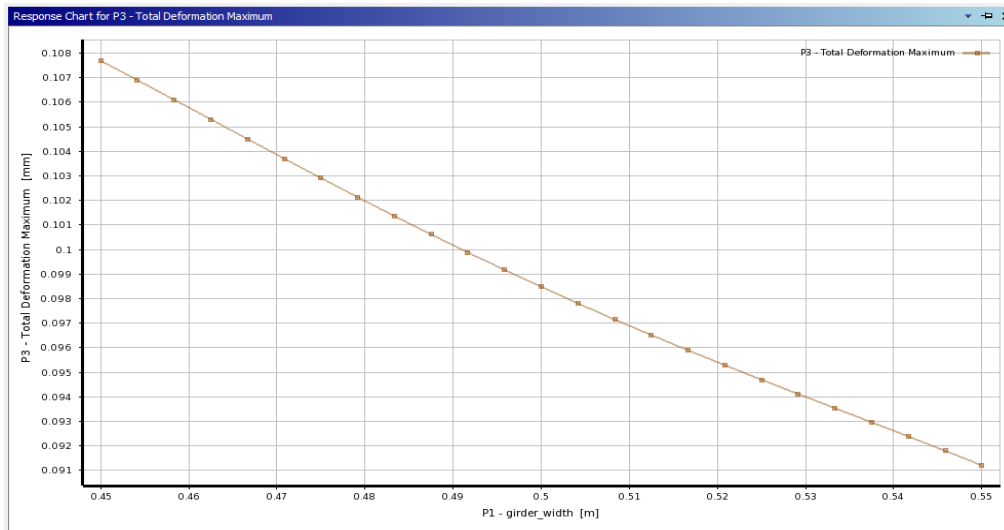
Figure 5.21: Variation of 1st freq. deformation vs "girder_width"

The 1st frequency deformation reduces linearly with increase in "girder_width" . The least deformation is obtained for .55m "girder_width" and max. value of deformation is obtained for .45m "girder_width".
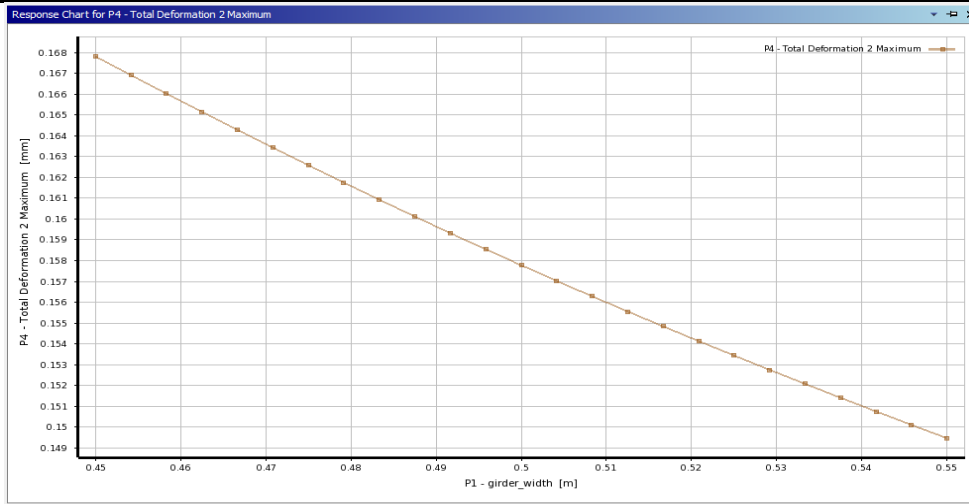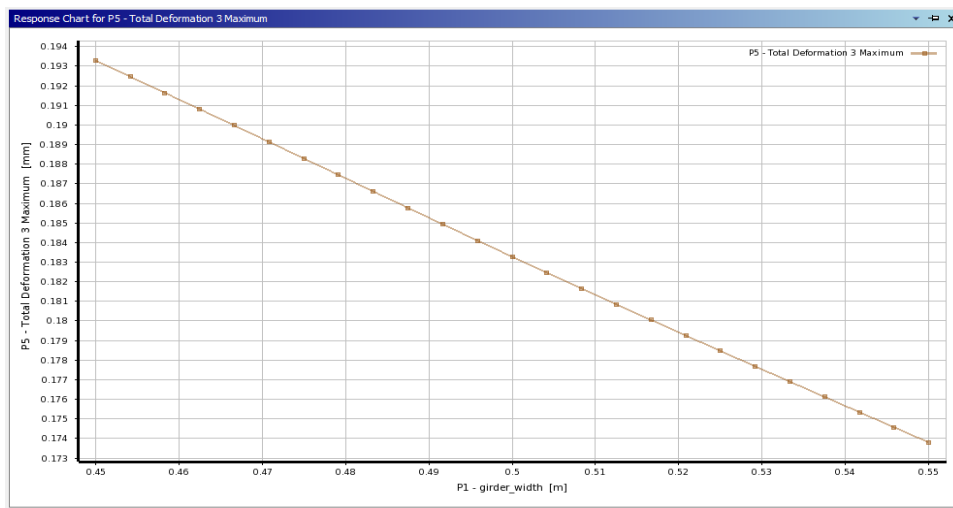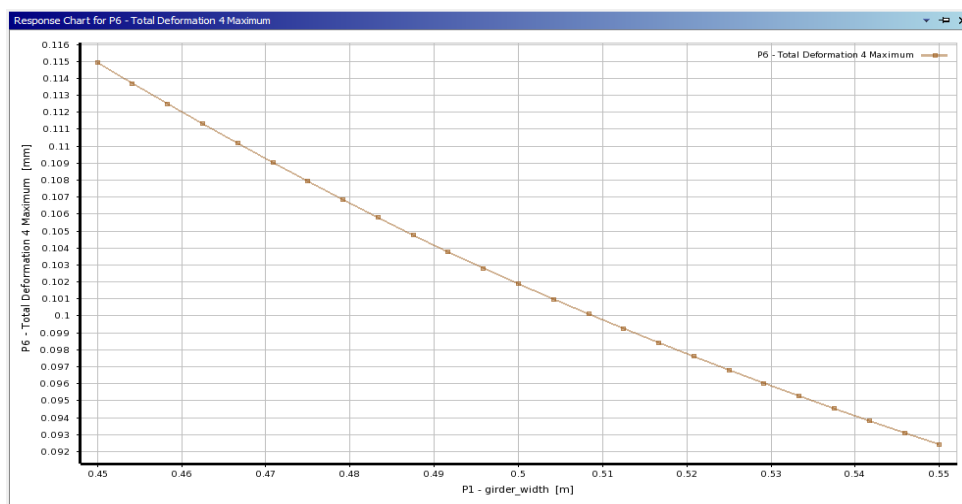
Figure 5.22: Variation of 2nd freq. deformation vs "girder_width"

The 2nd frequency deformation reduces linearly with increase in "girder_width". The least deformation is obtained for .55m "girder_width" and max. value of deformation is obtained for .45m "girder_width".
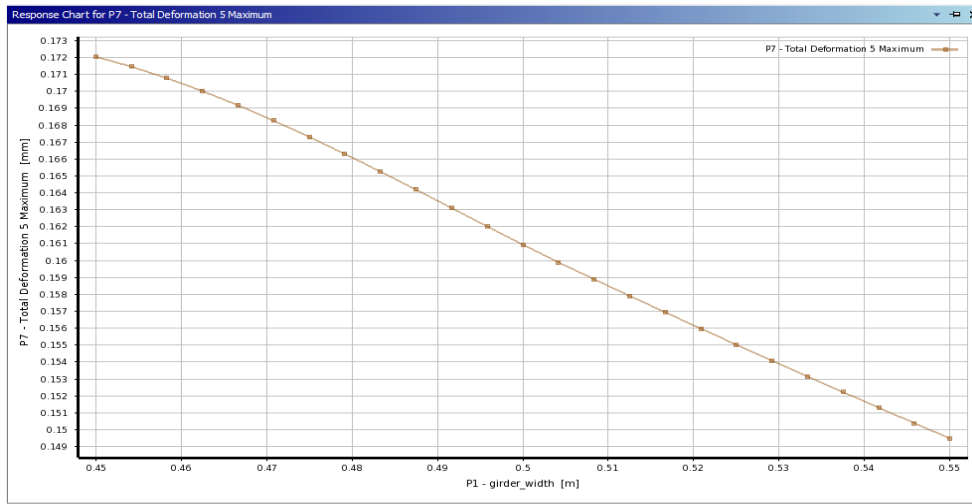

Figure 5.23: Variation of 3rd freq. deformation vs "girder_width"

The 3rd frequency deformation reduces linearly with increase in "girder_width" . The least deformation is obtained for .55m "girder_width" and max. value of deformation is obtained for .45m "girder_width".

Figure 5.24: Variation of 4th freq. deformation vs "girder_width"

The 4th frequency deformation reduces linearly with increase in "girder_width". The least deformation is obtained for .55m "girder_width" and max. value of deformation is obtained for .45m "girder_width".
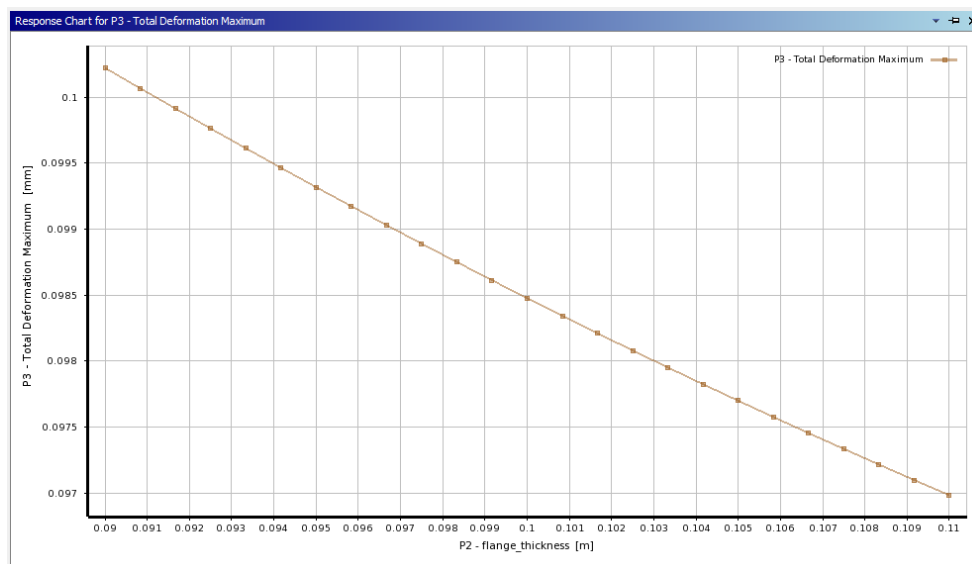

Figure 5.25: Variation of 5th freq. deformation vs "girder_width"

The 5th frequency deformation reduces linearly with increase in "girder_width" . The least deformation is obtained for .55m "girder_width" and max. value of deformation is obtained for .45m "girder_width".

Figure 5.26: Variation of 1st frequency deformation vs "flange_thickness"

The 1st frequency deformation reduces linearly with increase in "flange_thickness". The max. deformation is obtained for .09m "flange_thickness" and min. value of deformation is obtained for .11m "flange_thickness".
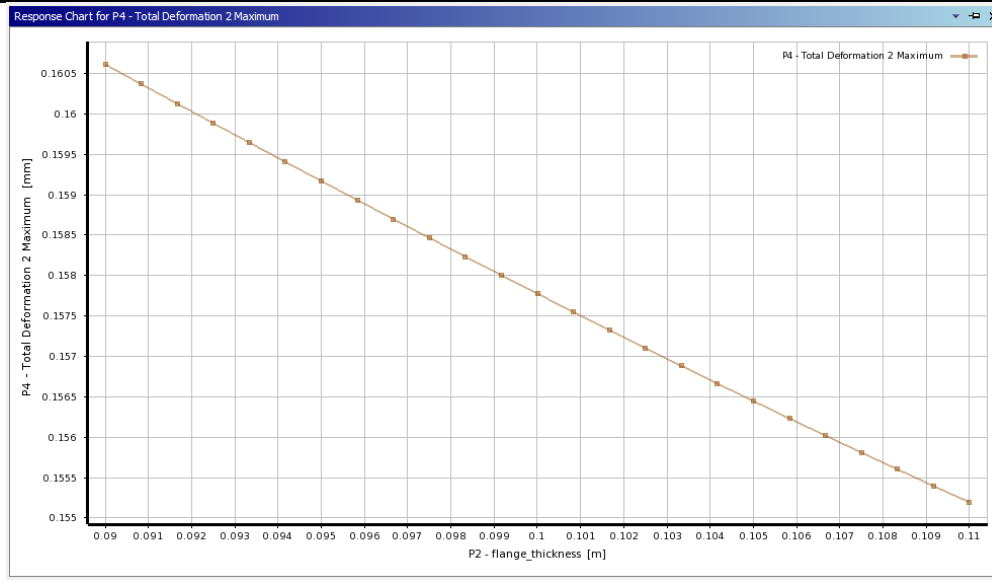
Figure 5.27: Variation of 2nd frequency deformation vs "flange_thickness"

The 2nd frequency deformation reduces linearly with increase in "flange_thickness". The max. deformation is obtained for .09m "flange_thickness" and min. value of deformation is obtained for .11m "flange_thickness".
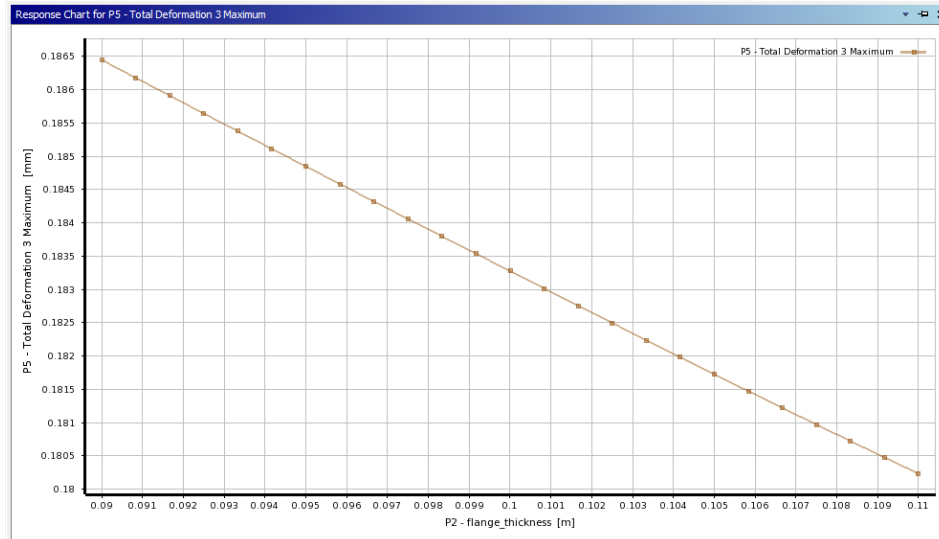

Figure 5.28: Variation of 3rd frequency deformation vs "flange_thickness"

The 3rd frequency deformation reduces linearly with increase in "flange_thickness". The max. deformation is obtained for .09m "flange_thickness" and min. value of deformation is obtained for .11m "flange_thickness".
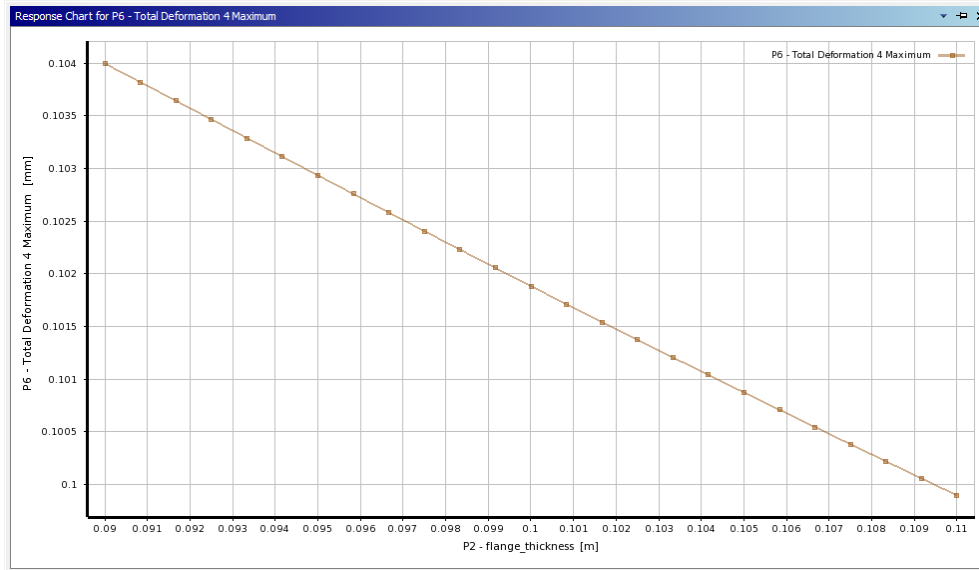
Figure 5.29: Variation of 4th frequency deformation vs "flange_thickness"

The 4th frequency deformation reduces linearly with increase in "flange_thickness". The max. deformation is obtained for .09m "flange_thickness" and min. value of deformation is obtained for .11m "flange_thickness".
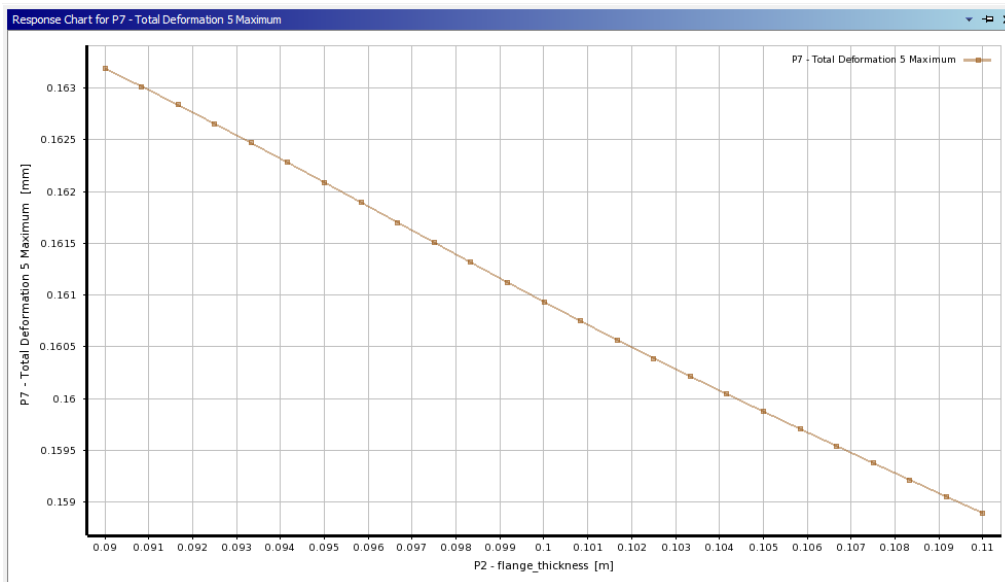

Figure 5.30: Variation of 5th frequency deformation vs "flange_thickness"

The 5th frequency deformation reduces linearly with increase in "flange_thickness". The max. deformation is obtained for .09m "flange_thickness" and min. value of deformation is obtained for .11m "flange_thickness".
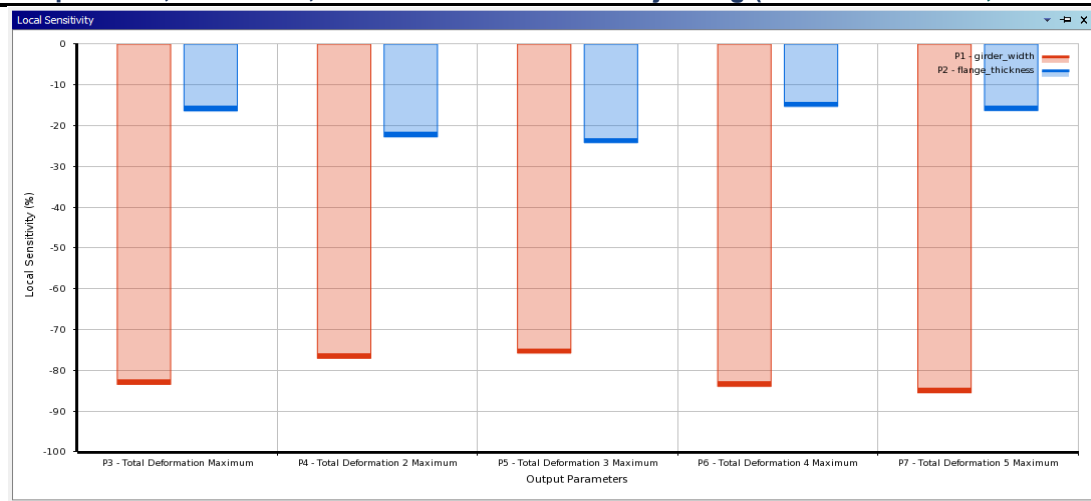
Figure 5.31: Sensitivity percentage comparison plot

Multiple sensitivity graphs for "girder_width" and "flange_thickness" are generated to analyse the first, second, third, fourth, and fifth frequency deformations. The graph presented above demonstrates that all frequencies have negative sensitivities. This implies that an increase in the values of these variables would result in a decrease in the deformation of all five natural frequencies, and conversely.

"Girder_width" has a higher sensitivity% of 83.45 compared to "flange_thickness" for the first frequency deformation, whereas lower sensitivity percentage of 16.39, indicating that "girder_width" has a greater impact on first-frequency deformation.

For 2nd frequency deformation, the "flange_thickness" has a lower sensitivity % of 22.75 compared to the "girder_width's" larger sensitivity percentage of 77.06, indicating that the "girder_width" has a greater impact on first frequency deformation.

For 3rd frequency deformation, the larger sensitivity % of 75.77 for the "girder_width" and the lower sensitivity percentage of 24.15 for the "flange_thickness", the former has a greater impact on first frequency deformation while the latter has less of an impact on 3rd frequency deformation.

The "flange_thickness" has a lower sensitivity% for fourth natural frequency deformation (15.28) than the "girder_width's" higher sensitivity% (83.94). This means that the "girder_width" has a bigger effect on first frequency deformation.

The "flange_thickness" for the fifth natural frequency deformation displays a lower sensitivity percentage of 16.28. compared to the "girder_width's" larger sensitivity percentage of 85.51, which indicates that the "girder_width" has a greater impact on first frequency deformation.

5.4   Crack Variables Effect on vibration characteristics

Taguchi Design of Experiments is used to optimise the response surface of a bridge with a broken I-girder. Using a central composite design method, the design parts are made up of many different numbers of "crack_minor" and "crack_major". FEA methods are used to figure out the amount of displacement for the first, second, third, fourth, and fifth natural frequencies. In columns D, E, F, G, and H, you can see the numbers for how much the shape has changed.

Table of Schematic B2: Design of Experiments (Central Composite Design : Auto Defined)

	A	B	C	D	E	F	G	H
1	Name	P8 - crack_minor (m)	P9 - crack_major (m)	P3 - Total Deformation Maximum (mm)	P4 - Total Deformation 2 Maximum (mm)	P5 - Total Deformation 3 Maximum (mm)	P6 - Total Deformation 4 Maximum (mm)	P7 - Total Deformation 5 Maximum (mm)
2	1 DP 0	0.018	0.09	0.099135	0.1586	0.18394	0.10233	0.16061
3	2	0.0162	0.09	0.099089	0.15859	0.18395	0.10231	0.16062
4	3	0.0198	0.09	0.098788	0.15842	0.18396	0.10212	0.16076
5	4	0.018	0.081	0.099217	0.15864	0.18392	0.10242	0.16064
6	5	0.018	0.099	0.099065	0.15856	0.18393	0.10235	0.16064
7	6	0.0162	0.081	0.098792	0.15841	0.18395	0.10219	0.16073
8	7	0.0198	0.081	0.098952	0.1585	0.18395	0.10224	0.16073
9	8	0.0162	0.099	0.099241	0.15863	0.18389	0.10243	0.16057
10	9	0.0198	0.099	0.098743	0.1584	0.18396	0.1021	0.16076

Figure 5.32: DOE chart for cracked bridge

Table of Schematic B3: Response Surface: Tolerances

	A	B	C
1	Name	Calculated Minimum	Calculated Maximum
2	P3 - Total Deformation Maximum (mm)	0.098739	0.099245
3	P4 - Total Deformation 2 Maximum (mm)	0.1584	0.15864
4	P5 - Total Deformation 3 Maximum (mm)	0.18388	0.18397
5	P6 - Total Deformation 4 Maximum (mm)	0.1021	0.10253
6	P7 - Total Deformation 5 Maximum (mm)	0.16056	0.16076

Figure 5.33: Max. and min. values of first 5 frequencies for cracked bridge
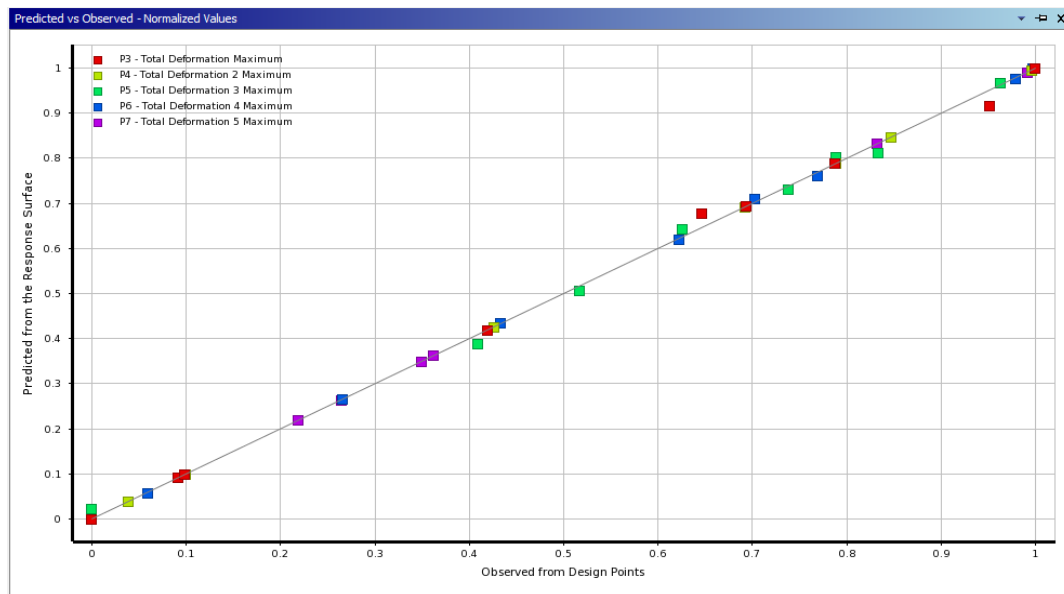

Figure 5.34: Statistical chart representing goodness of fit curve

Figure 5.34 shows the goodness-of-fit graph for figuring out how to make the bridge work best with different crack sizes. The observed value is shown by shaded circles that show the measured values of displacement at different natural rates. The expected value, based on a linear regression model, is shown by a straight line. The goodness of fit graph shows that the measured values (cells) are close to the expected values (straight line) when there is less spread in the goodness of fit plot.
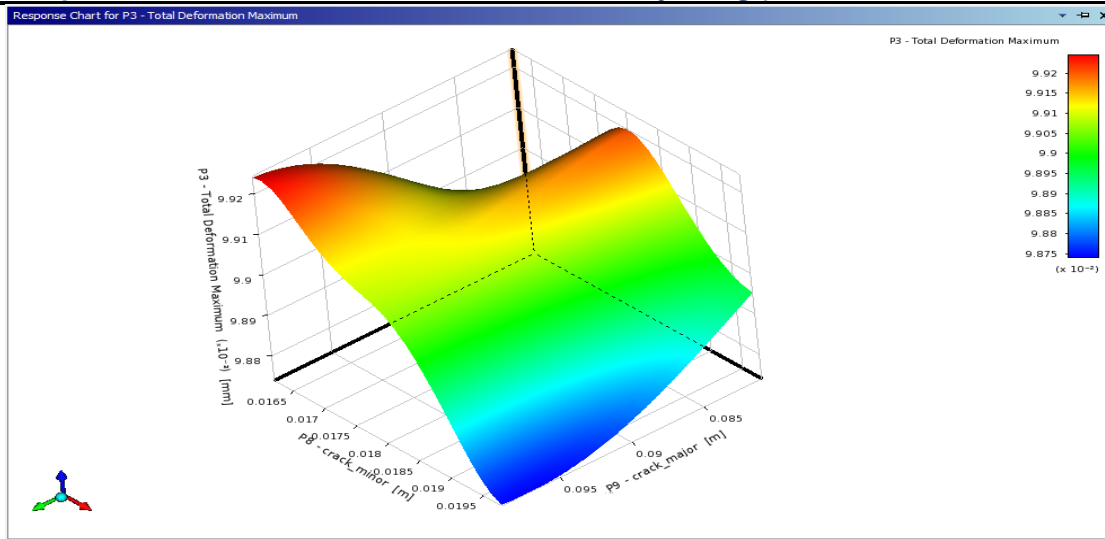
Figure 5.35: RSM plot of 1st frequency deformation vs "crack_minor" and "crack_major"

The range of values are determined for 1th frequency deformation. From the RSM plot shown in figure 5.35, the max. values of deformation are represented in red colour and min. values are represented in dark blue coloured region.

Table 5.8: RSM data of max. 5th frequency total deformation

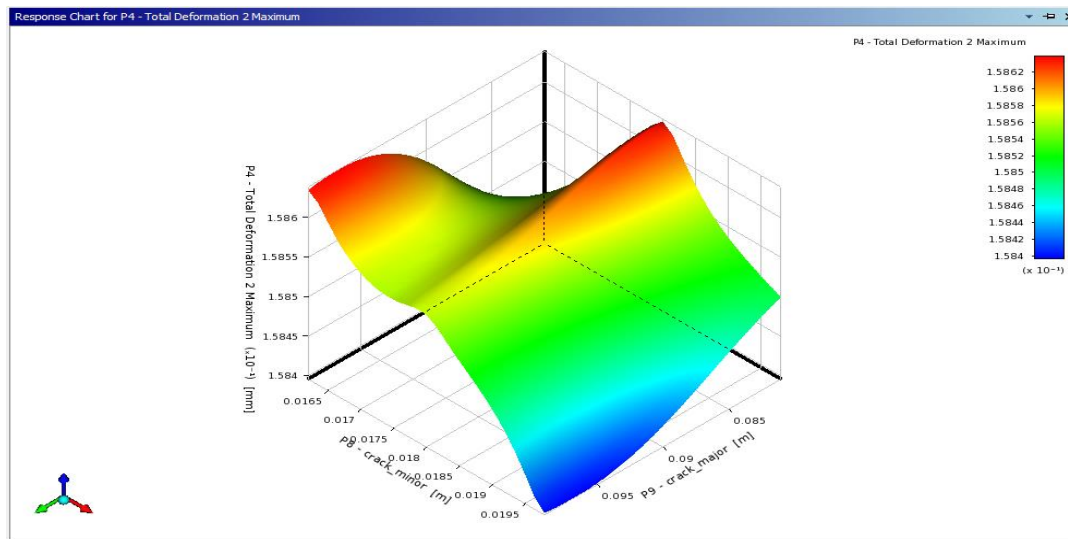| Crack_minor range	.092mm to .098mm
Crack_major range	.082mm to .089mm

Figure 5.36: RSM plot of 2nd frequency deformation vs "crack_minor" and "crack_major"

The range of values are determined for 2nd frequency deformation. From the RSM plot shown in figure 5.36, the max. values of deformation are represented in red colour and min. values are represented in dark blue coloured region.

Table 5.9: RSM data of max. 5th frequency total deformation

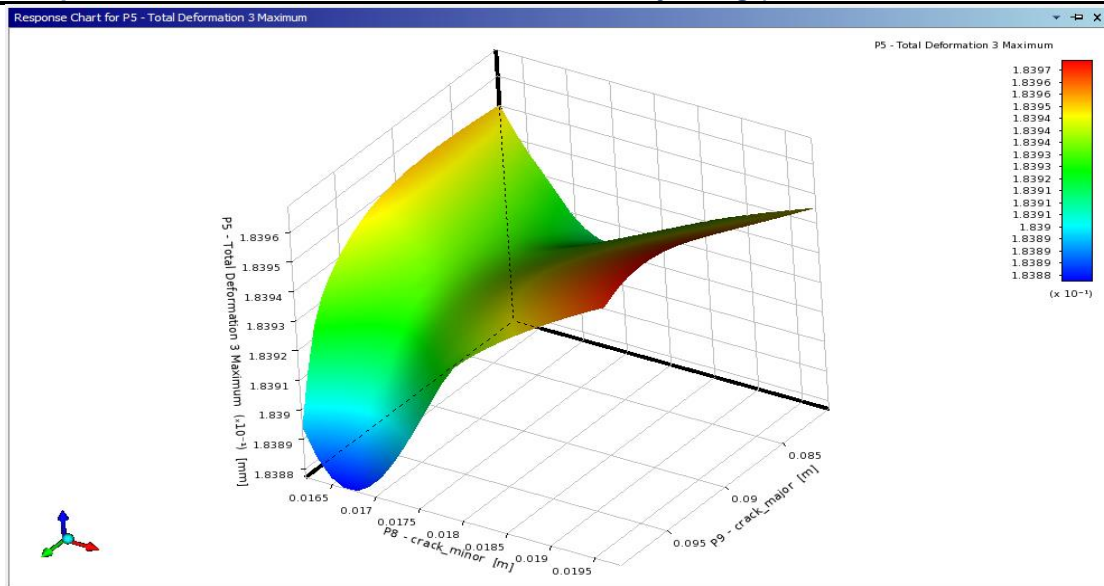| Crack_minor range	.09mm to .098mm
Crack_major range	.082mm to .089mm

Figure 5.37: RSM plot of 3rd frequency deformation vs "crack_minor" and "crack_major"

The range of values are determined for 3rd frequency deformation. From the RSM plot shown in figure 5.37, the max. values of deformation are represented in red colour and min. values are represented in dark blue coloured region. The least distorted regions are those that are highlighted by the dark blue area

Table 5.10: RSM data of max. 3rd frequency total deformation

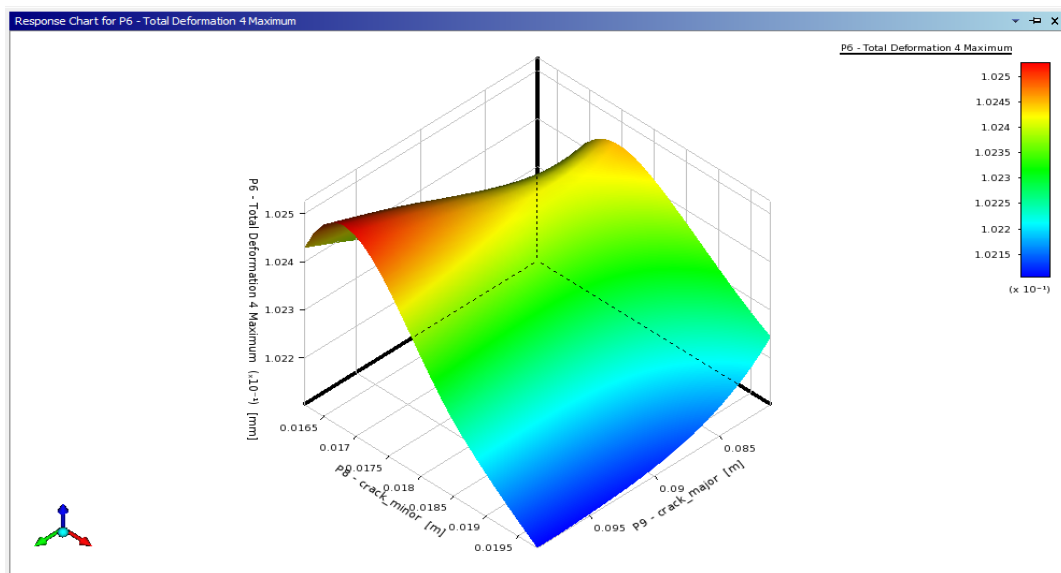| Crack_minor range	.0185mm to .0195mm
Crack_major range	.083mm to .098mm

Figure 5.38: RSM plot of 4th frequency deformation vs "crack_minor" and "crack_major"

The range of values are determined for 4th frequency deformation. From the RSM plot shown in figure 5.38, the max. values of deformation are represented in red colour and min. values are represented in dark blue coloured region.

Table 5.11: RSM data of max. 3rd frequency total deformation

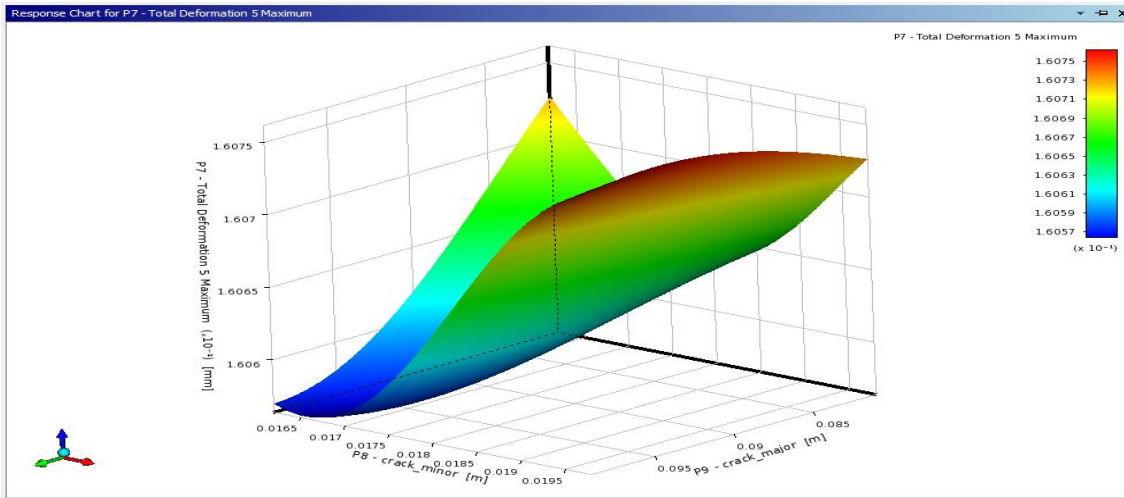| Crack_minor range	.0165mm to .0175mm
Crack_major range	.088mm to .098mm

Figure 5.39: RSM plot of 5th frequency deformation vs "crack_minor" and "crack_major"

The range of values are determined for 5th frequency deformation. From the RSM plot shown in figure 5.39, the max. values of deformation are represented in red colour and min. values are represented in dark blue coloured region.

Table 5.12: RSM data of max. 5th frequency total deformation

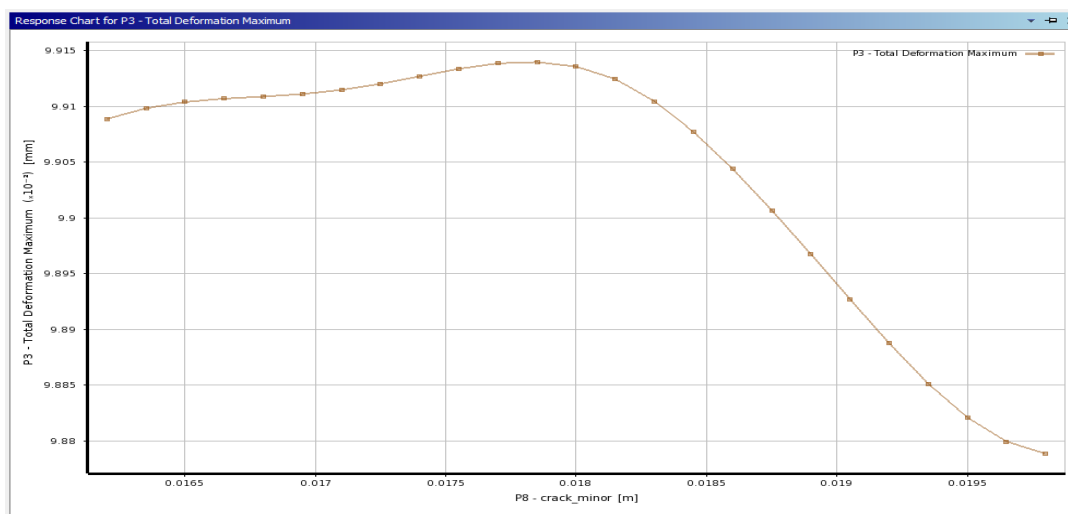| Crack_minor range	.019mm to .0195mm
Crack_major range	.082mm to .098mm

Figure 5.40: Variation of 1st freq. deformation vs "crack_minor"

The change in the first frequency as a function of the "crack_minor" dimension is almost constant for a "crack_minor" dimension of.0179m, and then it goes down in a linear way until it reaches its lowest value of.0195m. Figure 5.41 shows that the second frequency displacement has a similar structure.
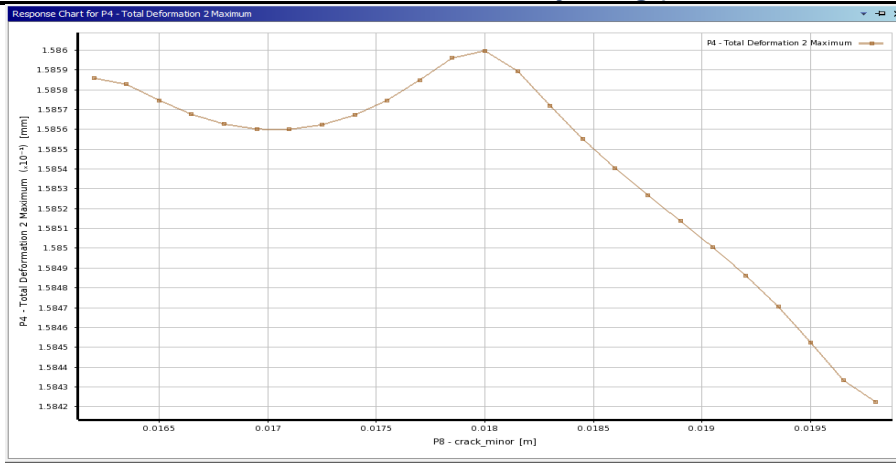
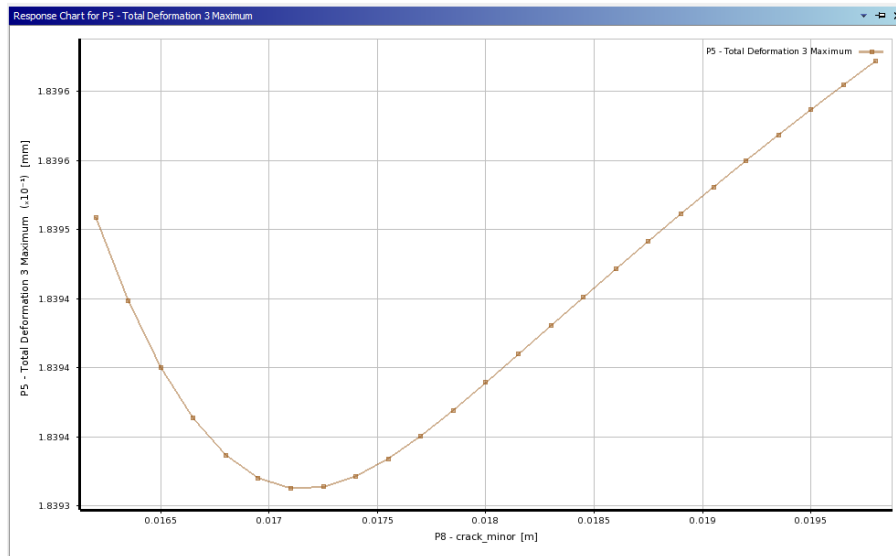Figure 5.41: Variation of 2nd freq. deformation vs "crack_minor"

Figure 5.42: Variation of 3rd freq. deformation vs "crack_minor"

For the third natural frequency, the displacement goes down until it reaches its minimum at a crack_minor dimension of .017m. After that, it goes up linearly until it reaches its maximum at a crack_minor dimension of .0195m.
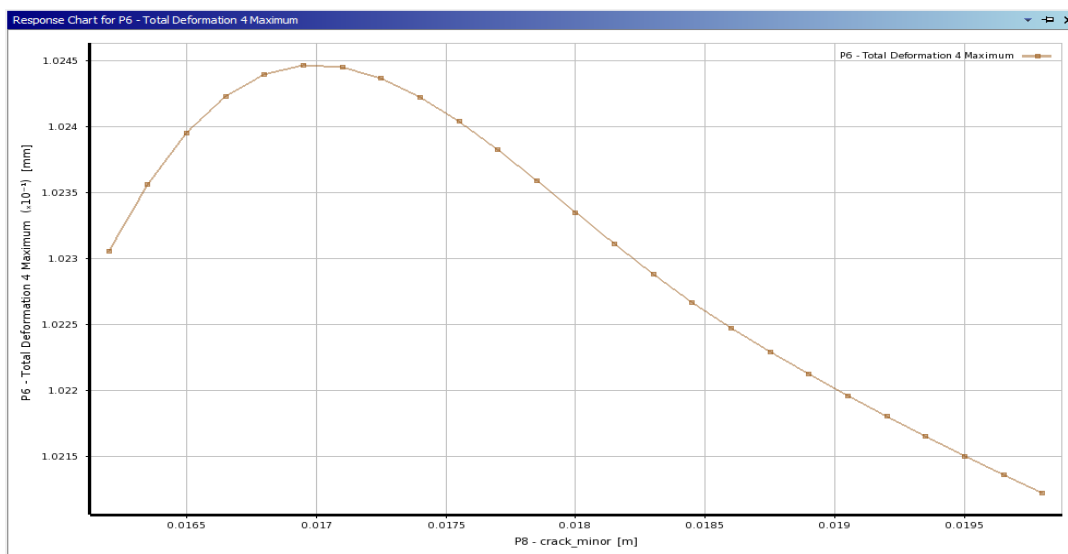

Figure 5.43: Variation of 4th freq. deformation vs "crack_minor"

For the fourth natural frequency, the displacement starts to go up and reaches its highest point when the crack_minor measurement is 0.017m. After that, it goes down in a straight line until it hits its lowest point at 0.0195m.
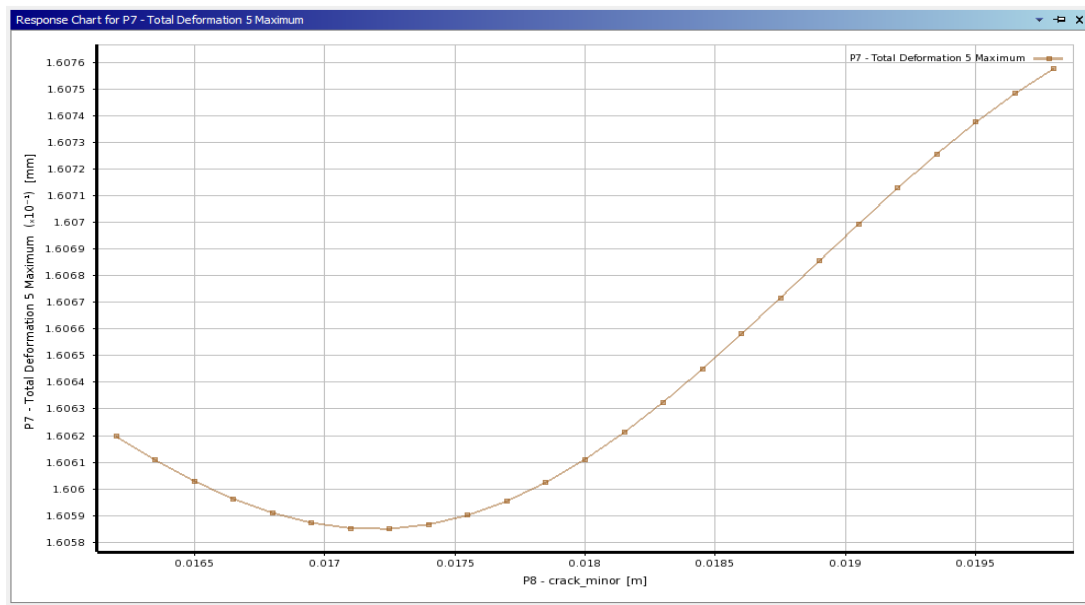

Figure 5.44: Variation of 5th freq. deformation vs "crack_minor"

For the fifth natural frequency, the distortion starts out small and grows linearly until it reaches its maximum value at a "crack_minor" size of.0195mm.
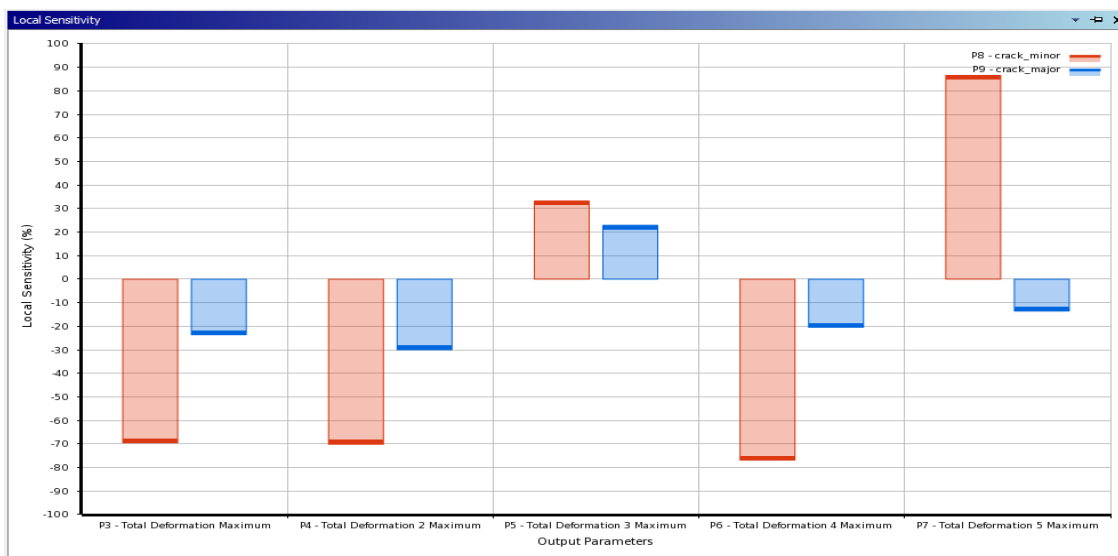
Figure 5.45: Sensitivity percentage comparison plot

For the "crack_minor" and "crack_major" dimensions, sensitivity graphs are generated and their influence on the output parameters is determined. The "crack_minor" dimension demonstrates negative sensitivity for the first and second frequencies, indicating that an increase in the "crack_minor" dimension results in an increase in the deformation of the first and second frequencies and vice versa.

For the first frequency deformation, the "crack_minor" dimension has a higher sensitivity rate (69.5%) than the "crack_major" dimension (23.61%). This means that the "crack_minor" dimension has a bigger effect on the first frequency deformation.

The sensitivity rate for second frequency deformation is higher for "crack_minor" dimension (70.1%), compared to "crack_major" dimension (29.9%). This means that "crack_minor" has a bigger effect on second frequency deformation.

The sensitivity percentage for 3rd frequency deformation is higher for "crack_minor" dimension (33.23%) than for "crack_major" dimension (22.92%). This means that "crack_minor" has a bigger effect on 3rd frequency deformation.

For fourth frequency deformation, "crack_minor" dimension is more sensitive (76.86%) than "crack_major" dimension (20.44%). This means that "crack_minor" has a bigger effect on fourth frequency deformation.

The sensitivity percentage for 5th frequency deformation is higher for "crack_minor" dimension (86.6%) than for "crack_major" dimension (13.54%). This means that "crack_minor" has a bigger effect on 5th frequency deformation.

CHAPTER- 6

CONCLUSION AND FUTURE SCOPE

6.1   Conclusion

FE computer simulation is an efficient technique for determining the vibrational properties of a bridge with I-shaped girders. The modal analysis performed on the straight bridge identifies the type and the extent of bridge deformation, in addition to providing crucial data on key areas and natural frequencies. The 1st response surface optimization technique is used to determine the effect of I shaped girder design variables on vibrational characteristics. Similarly, 2nd response surface optimization technique is used to determine the effect of crack dimensions on vibrational characteristics of bridge.

The detailed findings are: -

1. For the first frequency deformation, the "crack_minor" dimension has a higher sensitivity rate (69.5%) than the "crack_major" dimension (23.61%). This means that the "crack_minor" dimension has a bigger effect on the first frequency deformation.
2. The sensitivity rate for second frequency deformation is higher for "crack_minor" dimension (70.1%), compared to "crack_major" dimension (29.9%). This means that "crack_minor" has a bigger effect on second frequency deformation.
3. The sensitivity percentage for 3rd frequency deformation is higher for "crack_minor" dimension (33.23%) than for "crack_major" dimension (22.92%). This means that "crack_minor" has a bigger effect on 3rd frequency deformation.
4. For fourth frequency deformation, "crack_minor" dimension is more sensitive (76.86%) than "crack_major" dimension (20.44%). This means that "crack_minor" has a bigger effect on fourth frequency deformation.

5. The sensitivity percentage for 5th frequency deformation is higher for "crack_minor" dimension (86.6%) than for "crack_major" dimension (13.54%). This means that "crack_minor" has a bigger effect on 5th frequency deformation.

6. For first-frequency displacement, "girder_width" has a higher sensitivity% of 83.45 than "flange_thickness," whereas "flange_thickness" has a lower sensitivity% of 16.39, showing that "girder_width" has a bigger effect.

7. For 2nd frequency deformation, the "flange_thickness" has a lower sensitivity % of 22.75 compared to the "girder_width's" larger sensitivity percentage of 77.06, indicating that the "girder_width" has a greater impact on first frequency deformation.

6.2   Future Scope

The future scope of bridge vibration analysis holds immense potential for advancements in engineering and infrastructure development. With ongoing technological progress and increasing demand for safer and more efficient bridge designs, the field of bridge vibration analysis is expected to witness significant growth and innovation in the coming years.

One of the key areas of future development lies in the refinement of analytical techniques and methodologies used for bridge vibration analysis. Engineers will soon be able to precisely forecast and evaluate the dynamic behaviour of bridges subjected to a wide range of loading circumstances thanks to the continued development of sophisticated numerical models and simulation tools. More precise evaluations of bridge performance will be possible thanks to this, which will result in better designs and stronger structures.

In addition, new technology, such Internet of Things (IoT) sensors and real-time monitoring systems, will change the way bridge vibration analysis is conducted forever. With the help of these innovations, engineers will be able to continuously collect data on how bridges react to changing conditions, traffic patterns, and other dynamic impacts. Engineers may improve preventative maintenance plans, spot developing structural problems in real time, and take preventative action to lessen the dangers of excessive vibrations by analysing this plethora of data.

The investigation of new materials and building methods that might efficiently dampen bridge vibrations is another fruitful direction for future study. Engineers may create bridges that are naturally resistant to vibrations and offer greater resilience against dynamic loads by adding novel materials with better damping qualities or applying sophisticated building techniques. Such progress will aid in the construction of bridge structures that are both safer and more resilient to the effects of harsh conditions and can be maintained for the long term.

Furthermore, there is great potential for the use of AI and ML algorithms to the study of bridge vibrations. With the help of AI and ML, we can automate the study of massive datasets, which will speed up the process of spotting dangerous vibration patterns, installing early warning systems, and fine-tuning bridge designs. Engineers' ability to make decisions and progress towards intelligent, adaptive bridge systems would both benefit from this fusion.

REFERENCES:

[1]   S. Patel and U. Parekh, "Comparative Study of PSC . Tee Girder and PSC . Box Girder," *Int. J. Sci. Technol. Eng.*, vol. 2, no. 11, pp. 332–335, 2016.

[2]   P. D. P. Fahad P.P., "Analysis and Design of Post Tensioned Box Girder Bridge Using SAP," *Int ernat ional J. Sci. ific Res. Sci. Eng. Technol. IJSRSET J. T he INdIaN roads Congr.*, vol. 3, no. 2, pp. 2394–4099, 2017, [Online]. Available: http://www.engineeringcivil.com/analysis-and-design-of-prestressed-concrete-box-girder-bridge.html

[3]   P. Kumar, S. V. V. K. Babu, and D. Aditya Sai Ran, "Analysis and Design of Prestressed Box Girder Bridge," *Int. J. Constr. Res. Civ. Eng.*, 2016.

[4]   Ravikant and J. Chand, "Design and Analysis of Bridge Girders using Different Codes," *Int. J. Eng. Res. Technol.*, 2019.

[5]   Z. Xia, A. Li, J. Li, H. Shi, M. Duan, and G. Zhou, "Model updating of an existing bridge with high-dimensional variables using modified particle swarm optimization and ambient excitation data," *Meas. J. Int. Meas. Confed.*, 2020, doi: 10.1016/j.measurement.2020.107754.

[6]   Y. Y. PRIYA and T.SUJATHA, "COMPARATIVE ANALYSIS OF POST TENSIONED T-BEAM BRIDGE DECK BY RATIONAL METHOD AND FINITE ELEMENT METHOD," *Int. J. Res. IT, Manag. Eng.*, vol. 6, no. 09, pp. 1–13, 2016.

[7]   Sharu.E, N. M, and G. R. M, "Design of RCC t-beam bridge considering overloading due to congestion," *Indian J. Sci. Res.*, vol. 17, no. 12, pp. 211–216, 2018.

[8]   A. Ahmed and P. R. B. Lokhande, "COMPARATIVE ANALYSIS AND DESIGN OF T-BEAM AND BOX GIRDERS," *Int. Res. J. Eng. Technol.*, 2017.

[9]   S. Jha, C. Rajesh, and Srilaskmi, "Comparative Study of RCC Slab Bridge by Working Stress (IRC : 21-2000) and Limit State (IRC : 112-2011)," *Int. J. Mag. Eng. Technol. Manag. Res.*, vol. 2, no. 08, pp. 223–227, 2015.

[10]   P. Soni, "Review of Design Procedure for Box Girder Bridges," *Int. J. Res. Appl. Sci. Eng. Technol.*, 2017, doi: 10.22214/ijraset.2017.9278.

[11]   F. Chen, Z. jiang Du, M. Yang, F. Gao, W. Dong, and D. Zhang, "Design and analysis of a three-dimensional bridge-type mechanism based on the stiffness distribution," *Precis. Eng.*, 2018, doi: 10.1016/j.precisioneng.2017.07.010.

[12]   N. Le Chau, N. T. Tran, and T. P. Dao, "A Multi-response Optimal Design of Bridge Amplification Mechanism Based on Efficient Approach of Desirability, Fuzzy Logic, ANFIS and LAPO Algorithm," *Arab. J. Sci. Eng.*, 2020, doi: 10.1007/s13369-020-04587-3.

[13] A. M. B. Martins, L. M. C. Simões, and J. H. J. O. Negrão, "Optimization of cable-stayed bridges: A literature survey," *Adv. Eng. Softw.*, 2020, doi: 10.1016/j.advengsoft.2020.102829.

[14] S. Sabatino, D. M. Frangopol, and Y. Dong, "Sustainability-informed maintenance optimization of highway bridges considering multi-attribute utility and risk attitude," *Eng. Struct.*, 2015, doi: 10.1016/j.engstruct.2015.07.030.

[15] O. Skoglund, J. Leander, and R. Karoumi, "Optimizing the steel girders in a high strength steel composite bridge," *Eng. Struct.*, 2020, doi: 10.1016/j.engstruct.2020.110981.

[16] A. O. Thippeswamy, "Analysis of load optimization in cable stayed bridge using CSI bridge software," *Int. J. Appl. Eng. Res.*, vol. 13, pp. 78–80, 2018.

[17] Z. Wang, N. Zhang, X. Du, S. Wang, and Q. Sun, "Multiobjective Optimization of Cable Forces and Counterweights for Universal Cable-Stayed Bridges," *J. Adv. Transp.*, 2021, doi: 10.1155/2021/6615746.

[18] S. H. Huang, Y. H. Huang, C. A. Blazquez, and G. Paredes-Belmar, "Application of the ant colony optimization in the resolution of the bridge inspection routing problem," *Appl. Soft Comput. J.*, 2018, doi: 10.1016/j.asoc.2018.01.034.

[19] A. Kohansarbaz, A. Kohansarbaz, B. Yaghoubi, M. A. Izadbakhsh, and S. Shabanlou, "An integration of adaptive neuro-fuzzy inference system and firefly algorithm for scour estimation near bridge piers," *Earth Sci. Informatics*, 2021, doi: 10.1007/s12145-021-00652-z.

[20] H. K. Upadhyay and R. K. Raj, "Analysis of Critical Barriers in Bridge Construction using Best Worst Method," *Int. J. Eng. Res. Technol.*, vol. 9, no. 6, pp. 69–73, 2021.

[21] T. Wang, X. Guo, G. Long, and X. Liu, "Evaluation and Analysis of Bridge Modal Parameters Under Intelligent Monitoring Environment," *Front. Ecol. Evol.*, vol. 10, no. June, pp. 1–8, 2022, doi: 10.3389/fevo.2022.943865.

[22] S. Karimi and O. Mirza, "Damage identification in bridge structures: review of available methods and case studies," *Aust. J. Struct. Eng.*, vol. 24, no. 2, pp. 89–119, 2023, doi: 10.1080/13287982.2022.2120239.

[23] D. P. E. Gokul Mohandas V 1 and P.G., "A Review on Design and Analysis of Prestressed Concrete Bridges," *Int. J. Innov. Res. Sci. Eng. Technol.*, vol. 9, no. 4, pp. 136–139, 2020, [Online]. Available: http://www.iaetsdjaras.org/gallery/1-august-jaras-2018.pdf

[24] K. Senthil, R. A. Khan, S. Arvin, and A. Singh, "Structural Behavior of Railway Bridges Against Wheel Loading by Finite Element Analysis," *Int. J. Struct. Eng. Anal.*, vol. 3, no. 1, pp. 1–14, 2017, [Online]. Available: www.journalspub.com

[25] A. Jain and , Dr. J.N. Vyas, "Modal Analysis of Bridge Structure Using Finite Element Analysis," *IOSR J. Mech. Civ. Eng.*, vol. 13, no. 04, pp. 06–10, 2016, doi: 10.9790/1684-1304040610.

[26] Z. Zheng and Y. Bai, "Effects of Impact Loads on Mechanical Performance for Truss Structure," *World J. Eng. Technol.*, vol. 05, no. 03, pp. 135–140, 2017, doi: 10.4236/wjet.2017.53b015.

[27] O. Md. Emdadul Hoque Ferdous, "AN INVESTIGATION OF THE BEHAVIOR OF MECHANICAL STRUCTURES DUE," *Proc. Int. Conf. Mech. Eng. Renew. Energy, 2017*, no. December, 2017.

[28] H. Wang, H. Gao, and S. Qin, "Fatigue performance analysis and experimental study of steel trusses integral joint based on multi-scale FEM," *Eng. Rev.*, vol. 37, no. 3, pp. 257–262, 2017.

[29] T. J. Jayakrishnan and L. P. R, "Analysis of Seismic Behaviour of a Composite Bridge using ANSYS," *Int. J. Eng. Res. Technol.*, vol. 6, no. 05, pp. 473–475, 2017.

[30] T. Gupta and M. Kumar, "Flexural response of skew-curved concrete box-girder bridges," *Eng. Struct.*, vol. 163, pp. 358–372, 2018, doi: 10.1016/j.engstruct.2018.02.063.

[31] R. Wodzinowski, K. Sennah, and H. M. Afefy, "Free vibration analysis of horizontally curved composite concrete-steel I-girder bridges," *J. Constr. Steel Res.*, vol. 140, pp. 47–61, 2018, doi: 10.1016/j.jcsr.2017.10.011.

[32] M. Avalle, G. Chiandussi, and G. Belingardi, "Design optimization by response surface methodology: application to crashworthiness design of vehicle structures," *Struct. Multidiscip. Optim.*, vol. 24, no. 4, pp. 325–332, 2002, doi: 10.1007/s00158-002-0243-x.

[33] A. Y. Aydar, "Utilization of Response Surface Methodology in Optimization of Extraction of Plant Materials," *Stat. Approaches With Emphas. Des. Exp. Appl. to Chem. Process.*, no. March, 2018, doi: 10.5772/intechopen.73690.